OPTICAL IMAGING AND MEASURING METHODS TO ASSESS PORCINE KIDNEY MICROCIRCULATION DURING NORMOTHERMIC MACHINE PERFUSION

- a comparative proof-of-concept study -

Tom, Teeuwen

Student number : 4544366

29 July 2022

Thesis in partial fulfilment of the requirements for the joint degree of Master of Science in

Technical Medicine

Leiden University ; Delft University of Technology ; Erasmus University Rotterdam

Master thesis project (TM30004 ; 35 ECTS)

Dept. of Biomechanical Engineering, TUDELFT

December 2021 – August 2022

Supervisor(s):

Prof. dr. ir. Ian Alwayn, LUMC

Dr. Jason Doppenberg, LUMC

Dr. Volkert Huurman, LUMC

Dr. Dorottya de Vries, LUMC

Thesis committee members:

Prof. dr. ir. Ian Alwayn, LUMC (chair)

Dr. Jason Doppenberg, LUMC

Dr. Dorottya de Vries, LUMC

Prof. dr. Gijs van Soest, Erasmus MC

Abstract

OBJECTIVE This study aims to compare non-invasive real-time optical imaging and measuring methods for the quantification of microcirculation of organs during normothermic machine perfusion (NMP). This could help to determine which method is most promising for further development towards a clinical objective transplantability assessment tool.

BACKGROUND In organ transplantation, microvascular damage due to an ischemic period and reperfusion is inevitable. Evidence suggests a correlation between microcirculation during reperfusion and post-implantation organ functionality. Optical methods can measure the organ microcirculation in real-time in-vivo. Laser Speckle Contrast Imaging (LSCI), Near Infrared Spectroscopy (NIRS) and Sidestream Dark Field Imaging (SDFI) were evaluated on this purpose during NMP of porcine slaughterhouse kidneys.

METHODS An experiment consisting of steady-state NMP and intervention phases was designed. In the intervention phases, the pressure control was decreased and increased in steps and a main branch of the arteria renalis was clamped for three periods with each a consecutive reperfusion phase. Moreover, conventional functionality assessments, such as perfusate analysis, were performed. The microcirculations of the kidneys were imaged or measured with one of the optical methods throughout the experiment.

RESULTS Consistent responses to the interventions were observed in the LSCI signals. Moreover, some significant correlation was found between these signals and conventional functionality assessments. The signals measured with NIRS showed some trend in response to the interventions. However, these were not as consistent as in the LSCI signals. SDFI recordings were blurred and did not show any response to the interventions.

CONCLUSIONS From comprehension of the methods by (semi-)objective metrics, it can be concluded that LSCI is the most promising method for further development towards a clinical objective transplantability assessment tool. Significant correlations that were found between the LSCI signals and conventional functionality assessments were considered not clinically relevant due to the small sample size and limited comprehension between different experiments.

Introduction

Blood circulation delivers nutrients and oxygen to cells and carries waste materials away, which is essential for cellular metabolism (1). Temporary absence of blood circulation is inevitable during cold organ preservation in the ischemic period between explantation and implantation in transplantation procedures (2). This period initiates a cascade of biological reactions, for example, ATP depletion (3), the activation of xanthine oxidase (4), and the generation of radical oxygen species (5). These reactions lead to postischemic cellular effects such as endothelial cell dysfunction (6), impaired vasodilatation (7), and enhanced vasoconstriction (8), which could damage the organ tissue and deteriorate its functionality.

Although timely post-ischemic reperfusion is needed to limit these effects, the reperfusion could further damage the ischemic tissue (9). Therefore, the presence of blood flow into an organ on a macroscopic level during reperfusion is not necessarily related to a good clinical outcome. Local microcirculation can be absent under a total blood inflow within a physiological range, for instance, due to endothelial swelling induced by hypoxia during cold preservation (10, 11) and inflammatory reactions induced by reperfusion (8). Evidence suggests a correlation between microcirculation during reperfusion and post-implantation organ functionality, for example, in renal (12) and pancreatic grafts (13, 14). Moreover, prolonged cold preservation times have been associated with both microvascular impairment and poor clinical outcomes (15-17).

The expected functionality of a donor organ is considered to decide whether to implant a graft or not (18). However, downregulation of cellular metabolism during static cold storage (SCS) imposes restraints on the organ functionality assessment (19). Ex-vivo perfusion machines, which can be categorized into hypothermic machine perfusion (HMP) and normothermic machine perfusion (NMP), are currently considered to support the organ functionality assessment (20). During HMP, oxygen-containing perfusate at temperatures below 12°C is pumped through the organ to restore the tissue oxygen saturation and restart the aerobe ATP formation in the mitochondria (21). Biomarker levels in the perfusate can be monitored during HMP to predict post-transplant outcomes. However, a correlation between biomarkers and these outcomes has only been found for flavin mononucleotide (FMN) in liver grafts, which is a small molecule produced during nicotinamide adenine dinucleotide (NADH) oxidation (22). In kidney grafts, no correlation between HMP biomarkers and post-transplant outcomes has been found yet (23). NMP can be started directly after organ retrieval, or after a period of SCS or HMP. During NMP, a perfusate containing erythrocytes and oxygen at 37 °C is pumped through the organ's vasculature to recover the cellular energy status, to allow repair of reversible injury and to facilitate organ functionality assessment (20). This assessment is especially valuable during end-ischemic NMP, since it is likely that biological reactions to a prior SCS period cause reperfusion injury (24).

Organ functionality assessments can be based on organ-specific biomarkers. For instance, ASAT, ALAT, and biliary HCO_3^-, pH and glucose, have been verified as liver quality indicators during NMP (25-28). However, for kidney grafts, an objective assessment is lacking. *Hosgood et al.* developed an NMP assessment score consisting of the macroscopic appearance of the kidney, renal blood flow (RBF) and total urine output (29). Although this score has been verified for assessment of quality and transplantability before transplantation, its parameters are subjective and can be manipulated by changing the perfusion conditions. So far, no objective method to assess the functionality and transplantability of donor organs during NMP has been verified. Imaging and measuring techniques could provide real-time assessments that could help professionals to make instant decisions. Currently, these decisions are based on time-consuming periodic laboratory assessments, which can lead to missing sudden physiological changes.

Macroscopic imaging and measuring devices can quantify the amount of blood flow in tissues or organs (30, 31). The value of these techniques is limited since they cannot account for local differences in microcirculation (32). Techniques that image or measure local differences in microcirculation directly could add valuable information on the expected functionality of an organ after implantation (33). However, these techniques are not yet routinely deployed perioperatively in clinical transplantation procedures (34, 35).

Many imaging and measuring methods for microcirculation are impractical, time-consuming, or invasive. For instance, Magnetic Resonance Imaging (MRI) and Computed Tomography (CT) are usually not available near an operating room due to their size. Moreover, analysis with a transmitted light microscope takes time and cannot provide real-time in-vivo data (36). Some other imaging or measuring methods that can measure in real-time use fluorescent dyes, which can be appraised as invasive and unwanted for clinical use (37). These constraints hamper the implementation of these methods for

pre-operative organ assessment in transplantation procedures.

Optical imaging or measuring methods can visualise anatomic structures and measure functional characteristics by using a light source and photodetector (38). Tissues, cells and molecules have unique reactions to different light wavelengths and can influence the detected light by absorption, reflection, polarization and scattering (39). These biological reactions to light are the fundaments of the operation of optical imaging or measuring methods. Nowadays, these methods are particularly used for percutaneous measurement, for example, for the diagnosis of dermatologic conditions (40), diabetes (41), Raynaud's phenomenon (42), and fibromyalgia (43).

Many different optical methods that could be used to image or measure the microcirculation of donor organs during NMP are available for commercial use. The strengths and weaknesses of non-invasive real-time optical methods regarding transplantation surgery were assessed in a literature review (44). This review assembled 9 optical methods that have been used during periods of complete local circulatory arrest and immediately following reperfusion to resemble the periods of organ preservation and reperfusion. It was concluded that each method has its unique set of strengths and weaknesses and that Laser Speckle Contrast Imaging (LSCI) shows the greatest potential in transplant surgery. Since some of the optical methods have not been used to image or measure during in-vivo or ex-vivo organ reperfusion, an objective assessment of the suitability of their use during NMP is lacking. Therefore, the purpose of this research is to compare these non-invasive real-time optical imaging and measuring methods for the quantification of microcirculation of organs during NMP. This could help to determine which method is most promising for further development towards a clinical objective transplantability assessment tool.

In the experiments of this research, exclusively the microcirculation of porcine slaughterhouse kidneys was assessed with LSCI, Near Infrared Spectroscopy (NIRS) and Sidestream Dark Field Imaging (SDFI). Kidneys were considered the best applicable organs for the experiments, since they did not require vessel reconstructions for ex-vivo perfusion, and expertise and materials for kidney perfusions were already available within the institute. Slaughterhouse porcine organs were chosen because of their wide availability, low costs, and physiology that approaches human physiology. LSCI, NIRS and SDFI were the only available methods of the 9 methods that were discussed in the literature review. Therefore, they were all included for further experimental research in this study.

Theoretical background

Although LSCI, NIRS and SDFI are all optical methods, their operation and the principles they are based on differ. LSCI is based on a dynamic speckle pattern that arises from constructive and destructive interference of polarized backscattered light after illumination of a region of interest by coherent red laser light (45). The speckle pattern is detected by a photodetector and depends on erythrocyte movement. Decreasing variation and increasing mean intensity in the speckle pattern indicate increasing perfusion. A polarization filter is located in front of the photodetector to minimize tissue surface reflections since these do not originate from erythrocyte movement. This filter transmits solely polarized light perpendicular to the illuminating beam (46).

A disadvantage of LSCI regarding the other two methods is the presence of a biological zero during complete circulatory arrest. Even when erythrocytes do not move through vessels in a region of interest (ROI) there is a signal measured, which is expected to be caused by residual Brownian movements of macromolecules (47, 48). Moreover, the LSCI signal is expressed in arbitrary units (AU) that cannot be translated to flow or velocity units (49). Therefore, inter-individual comparison of LSCI results is hard and can be unreliable. Theoretically, this problem does not impede intra-individual analyses, since a trend in the signal can be detected. However, some assumptions have to be made in each measurement to determine what signal can be attributed to normal perfusion levels.

The NIRS device used in the experiments (INVOS 7100, Medtronic) measures tissue oxygen saturation (StO_2). Measurements are based on differences in absorption rates of near-infrared (NI) light between oxygenated haemoglobin (HbO_2) and deoxygenated haemoglobin (HbH) (50, 51). The StO_2 can be calculated from the amount of detected NI light after emission through the tissue and is displayed as a percentage. Therefore, the measured signal can be used for reliable inter- and intra-individual analyses.

NIRS measures the StO_2 which differs from the arterial and venous saturation. The measured percentage represents an average saturation in the arteries, veins and capillaries in the path of the emitted light (52, 53). NIRS is widely used to measure cerebral oxygen saturation intra-operatively or in the intensive care unit. The INVOS 7100 exists out of 4 sensors that can be attached to the left and right forehead and the legs. Ischemic events can be detected by monitoring the cerebral and leg StO_2 with these sensors, for instance, events caused by malfunction of an extracorporeal

membrane oxygenation (ECMO) machine. *Kim et al.* found good agreement between the cerebral StO_2 and the jugular venous oxygen saturation and showed some agreement with a previously proposed intracerebral distribution of arterial and venous blood (52). Since StO_2 represents the venous oxygen saturation rather than the arterial oxygen saturation, signal decreases are caused by increased metabolism and therefore describe an improving situation.

SDFI devices use multiple light sources located in a circle at the bottom of a probe shaft to illuminate the tissue with polarized green light (54). This light is absorbed by haemoglobin in the capillaries and depolarized and backscattered by the surrounding tissue. Backscattered light orthogonal to a photosensitive camera in the probe shaft is detected after being filtered by an orthogonal polarizer. In this filter, reflected polarized light from superficial layers of the tissue is eliminated. The detected signal is processed into a video that visualises erythrocyte movement. Vessel density and perfusion can be assessed in these videos.

LSCI and SDFI were used on porcine slaughterhouse kidneys in experimental proof-of-concept research by *Heeman et al.* (55). They concluded that LSCI can image renal cortical microcirculation with high spatial and temporal resolution and detect local perfusion deficits. In the same research, they used SDFI to assess the perfusion simultaneously with LSCI. They removed the renal capsule locally to be able to image the renal cortical microcirculation. However, the limitations of imaging with an intact capsule were not discussed in this article. In clinical practice, the renal capsule cannot be removed during a transplantation procedure. Since this research assesses the potential of optical methods for further clinical development, the renal capsule was kept intact during the experiments.

In the literature review, the characteristics of these optical methods were assessed (44). Characteristics of optical methods were found to be divergent, although it was concluded that the tissue penetration depth of these methods is overall limited compared to non-optical imaging or measuring methods. For LSCI and SDFI, this depth is limited to approximately 1 mm (55, 56). However, the penetration depth of NIRS is an exception and can be up to a couple of centimetres in cerebral and leg measurements (53, 57). It was assumed that a similar penetration depth can be reached in renal measurements, which is advantageous when compared to LSCI and SDFI. However, no published articles describe the use of NIRS on organ tissue, thus proof does not exist yet.

Methods

A suitable optical method for quantification of microcirculation of kidneys during NMP possesses a high degree of differentiation for local differences in microcirculation. Also, changes in the microcirculation of different proportions must be indicated by the images or measurements. The research question that comprises the research purpose and these characteristics was: '*Which of the three optical imaging and measuring methods LSCI, NIRS and SDFI is the most feasible to assess the microcirculation of kidneys during NMP?'.*

An NMP experiment using porcine slaughterhouse kidneys was designed to help answer this research question. A protocol for the experiment was composed regarding the retrieval and preservation of the kidneys, the NMP setting, the interventions during the perfusion, the conventional functionality assessments, the optical imaging and measuring, and the analysis. For each optical imaging or measuring method, the experiment was repeated 2-3 times using kidneys from different pigs. Both right and left kidneys were included. The aim was to acquire a minimum of 2 successfully finished experiments for each optical method. However, 2 unsuccessful experiments or 1 successful and 1 unsuccessful experiment were considered satisfactorily for a method that showed significant limitations that made further experiments impossible or useless.

Retrieval and preservation

In two different slaughterhouses, kidneys were retrieved from pigs intended for consumption. These pigs were slaughtered by cutting the cervical vascular system. A minimum of 2 L of blood was collected in 1 L buckets filled with heparin (12 500 IU/L). The mixture of blood and heparin was transferred through a leucocyte filter and collected in a blood bag until 700 mL of leucocyte-depleted whole blood was collected. Hereafter, 1 g cefazoline in 10 mL aminoplasmal 10 % was added and the blood was stored at room temperature. In case the preservation duration was expected to be > 4 hours, 100 mL citrate phosphate glucose (CPG) buffer was added and the blood was stored at 4-12 °C. This buffer was custom-made and consisted of 2.99 g citric acid, 26.3 g sodium citrate, 2.22 g monobasic sodium phosphate and 6 g glucose, all dissolved in water for injection to make 1 L solution in total. The use of this buffer is expanded on in the text box '*Blood preservation'*.

After exsanguination of the pig, the carcass was placed in a hot water bath (°60 C) for approximately 60 min as is part of the slaughter

Blood preservation

Since erythrocytes in leucocyte-depleted whole blood are metabolically active at room temperature they are in demand of oxygen and nutrients, in particular glucose. When oxygen and glucose supplies are consumed, erythrocytes will get into distress leading to a release of lactate and potassium (58, 59). Irreversible damage and eventually cell death could threaten the usability of the perfusate during NMP. Glucose levels down to 2 mmol/L were measured after 3-4 hours of preservation at room temperature. Therefore, an alternative method was needed for preservations > 4 hours.

Two alternative blood preservation methods were invented for experimental research. These were oxygenated and glucose-infused preservation and preservation on a CPG buffer. Both methods were compared to untreated blood. All experiments were executed at room temperature with blood derived from one unique slaughterhouse pig.

For the oxygenated and glucose-infused preservation, the NMP system as can be seen in *figure 3* was used without the water bath, the infusion pump, and the kidney. The system was filled with 700 mL of leucocyte-depleted whole blood, which was pumped through the oxygenator by the centrifugal pump at 625 rpm. The carbogen supply (95 % CO_2, 5 % O_2) of the oxygenator was set at 0.5 L/min. Perfusate samples were taken 10 min before and 30, 150, 270, 360, and 900 min after the start of the oxygenated circulation. Directly after the sample at 30 min was taken, 15.2 g of glucose was added to the perfusate. Theoretically, this amount of glucose results in a glucose concentration equal to the concentration in the blood preserved on the CPG buffer.

For the preservation of whole blood on a CPG buffer, 14.3 mL of CPG buffer was added to 100 mL of leucocyte-depleted whole blood in a blood bag. This custom-made buffer consisted of 2.99 g citric acid, 26.3 g sodium citrate, 2.22 g monobasic sodium phosphate, and 25.5 g glucose, all dissolved in water for injection to make 1 L solution in total (60). Another 100 mL of leucocyte-depleted whole blood was stored in a blood bag without further treatment. Perfusate samples from both blood bags were taken 270 and 900 min after the moment the bags were filled, which was in parallel to the oxygenated and glucose-infused preservation.

Perfusate sample analysis with a blood gas analyser (RAPIDPoint 500, Siemens) was performed after the last sample was taken. To prevent a change in the parameters during the storage due to cell metabolism, plasm was isolated from one part of each sample. This part was used to analyse pH, glucose, potassium and lactate levels. The other part of the sample remained untreated and was used to analyse haemoglobin levels and the fractions oxygenated (FO2Hb) and deoxygenated haemoglobin (FHHb), methaemoglobin (FMetHb), and carboxyhaemoglobin (FCOHb). Potassium, lactate and haemoglobin were considered biomarkers of erythrocyte damage, glucose and FO2Hb biomarkers of metabolic activity, and FMetHb and FCOHb toxic biomarkers. All samples were stored at 7 °C.

A potassium level (*figure 2B*) of 7.88 mmol/L was measured in the blood before the start of the treatment. These levels remained stable in the untreated blood, while a decrease was observed in the CPG buffered blood. In the oxygenated and glucose-infused blood, the potassium levels could not be measured, which indicates an extraordinary high potassium level. The lactate level (*figure 2D*) was 4.61 mmol/L before the start of the treatment. In the untreated and oxygenated and glucose-infused blood, these levels slightly decreased in the first hours. However, the lactate levels had been increased to 8.24 mmol/L and 6.17 mmol/L respectively at 900 min. Lactate remained stable in the CPG buffered blood. Glucose levels (*figure 2C*) in the untreated blood decreased from 4.9 mmol/L to 1.2 mmol/L. Adding the CPG buffer to the blood resulted in a glucose level increase to nearly 40 mmol/L. In the oxygenated and glucose-infused blood, the glucose levels could not be measured after the glucose was added, which indicates an extraordinary high glucose level. In 900 min, the haemoglobin levels (*figure 2E*) decreased in all blood.

FMetHb and FCOHb (*figure 2F*) remained below 0.5 % in all samples, which is far below their toxic thresholds. In the oxygenated and glucose-infused blood, the FO2Hb level increased to nearly 100 % after the start of the treatment. The FO2Hb levels (*figure 2F*) remained stable between 60 and 80 % in the CPG buffered and untreated blood. However, after 900 min a slightly higher FO2Hb level was measured in the CPG buffered blood compared to the untreated blood.

In conclusion, the preservation of leucocyte-depleted whole blood on a CPG buffer was suggested as the best method for preservations > 4 hours. This preservation resulted in a pH (*figure 2A*) around 7.0, which can be corrected using NaHCO3 before the start of NMP. The most important observations in favour of the use of a CPG buffer were the decreasing potassium levels and the stable lactate levels. Although the haemoglobin level decreased to 7.4 mmol/L, probably caused by cellular damage, this level is considered sufficient for kidney NMP. The amount of glucose in the CPG buffer resulted in a glucose overshoot in the blood. Therefore, the amount of glucose in the CPG buffer was decreased from 25.5 g to 6 g for the kidney NMP experiments, which theoretically

resulted in a glucose level increase of 4 mmol/L. Lastly, the CPG buffered blood was stored at 4-12 °C during the experiments to decrease the metabolic activity of erythrocytes even further.

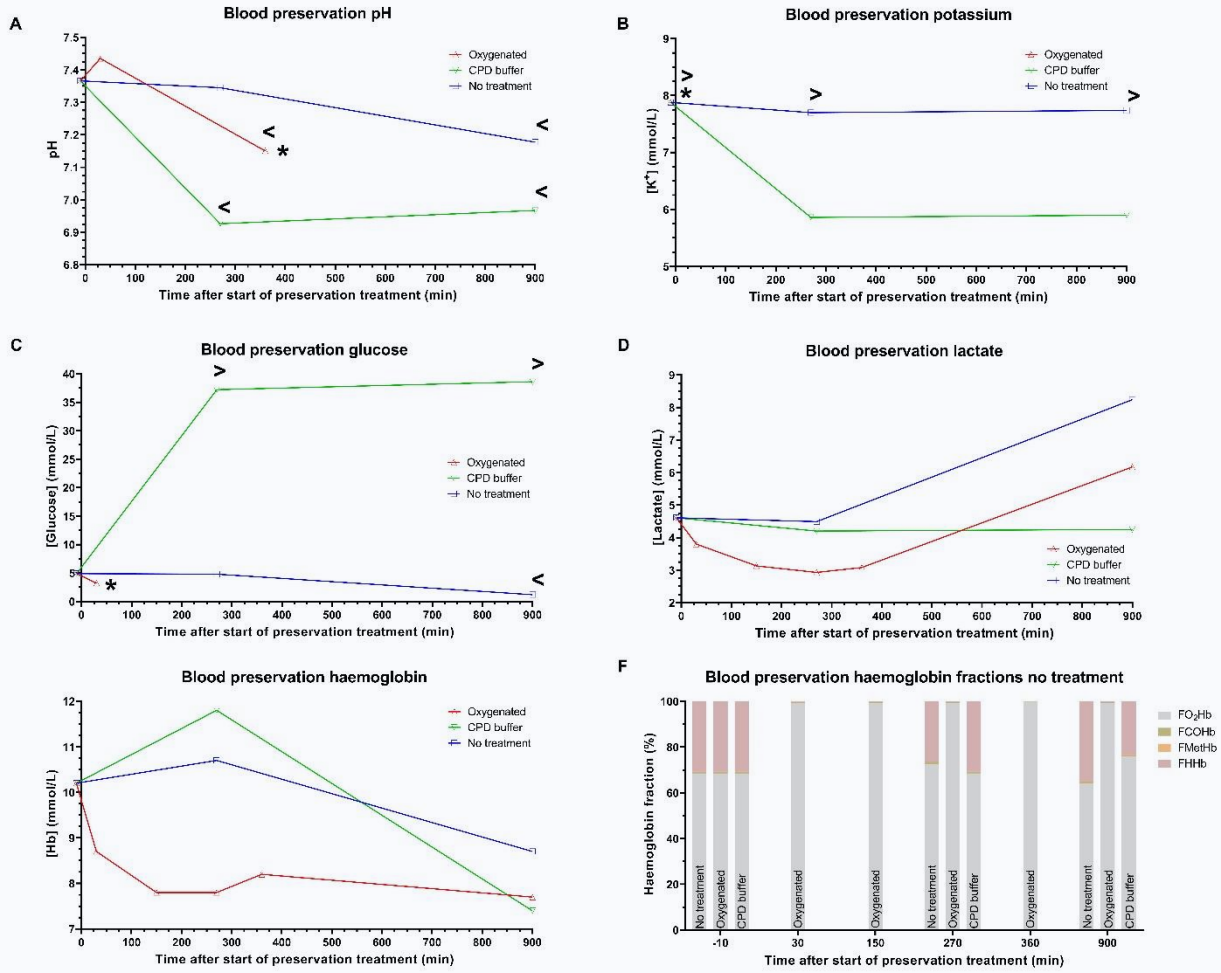

Figure 2

The pH (A), potassium (B), glucose (C), lactate (D), haemoglobin (E), and haemoglobin fractions (F) in the perfusate samples derived from the oxygenated and glucose-infused blood, the blood in a CPG buffer, and the untreated blood. * = The value of one or more perfusate parameter(s) could not be measured, < = The value of the perfusate parameter was much lower than the normal range and the device was not optimized for these values, > = The value of the perfusate parameter was much higher than the normal range and could be less reliable and the device was not optimized for these values.

procedure, whereafter the internal organs were cut out. The kidneys were separated from the other organs and the arteriae (aa.) renalis, venae (vv.) renalis and ureters were identified. To increase the chance of successful coupling to a perfusion machine, the aorta was preferably divided into a segment containing both arteries. Hereafter, the aorta could be split into two patches containing the artery origins that were used for cannulation. The vv. renalis and ureters were cut at the locations that left maximal length at the side of the kidney. After the retrieval of the kidney, the kidney with the best appearance was flushed with Ringers lactate at room temperature until the venous outflow was clear. Hereafter, the kidney was flushed with 200-500 mL University of Wisconsin Machine Perfusion Solution (UW-MPS) at 4 °C until the surface colour of the kidney stopped changing. In case more than 15 % of the kidney surface remained red or purple, the contralateral kidney was flushed as well following the same procedure. The warm ischemic time was noted.

The kidney that appeared to be the most viable was preserved using a pressure-controlled (25 mmHg), oxygenated (0.5 L/min) HMP roller pump system at 4-12 °C (*figure 1*). The system filled with UW-MPS was cooled, primed, and vented before the pig was slaughtered. UW-MPS was used

for the perfusion. After the kidney had been flushed, a 10-12 Fr arterial cannula was placed, fixated and connected to the HMP system and oxygenated perfusion was started. The start-time of oxygenated-HMP was noted and the kidney and blood were transported to the hospital. In case the planned preservation was > 4 hours, a water bath at 4 °C was attached to the oxygenator of the HMP system.

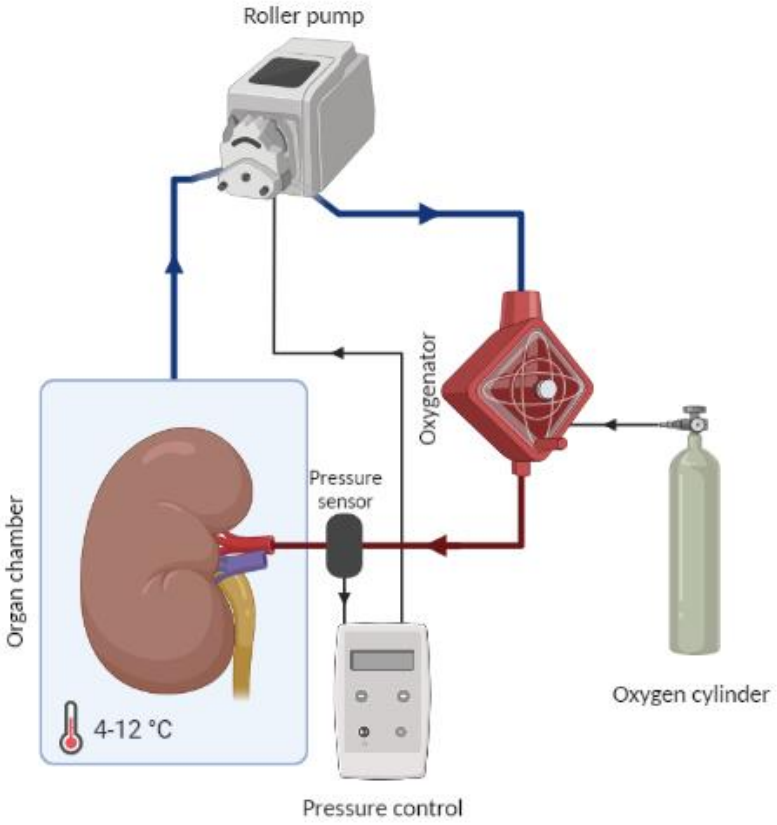

Figure 1
Schematic overview of the HMP system used for cold oxygenated preservation.

Normothermic machine perfusion

To finish the perfusate, 1 mmol creatinine in 1 mL aminoplasmal 10 % was added to the CPG buffered leucocyte-depleted whole blood in the blood bag. The NMP system (XVIVO, Groningen) as can be seen in *figure 3* was washed with sterile water at 37 °C. Hereafter, the system was filled with the perfusate and vented until all air bubbles were removed. The perfusate was oxygenated with carbogen (95 % O_2 and 5 % CO_2 at 0.5 L/min) and heated to 37 °C at least 30 min before the planned start of NMP. The pH, glucose level and osmolarity of the perfusate were set at their target values based on analysis of a sample taken directly after the oxygenation and temperature were set. For the analysis, a point of care blood gas analyser (i-STAT 1, Abbott or epoc NXS, Siemens) was used. To correct a pH lower than 7.35, sodium bicarbonate ($NaHCO_3$) 8.4 % was added according to the formulas:

$$\dots mL\ NaHCO_3\ 8.4\ \% = 10^{pH_d - PKA} \cdot 0.0307 \cdot pCO_2 - [HCO_3^-]$$

$$PKA = pH_c - \log\left(\frac{[HCO_3^-]}{0.0307 \cdot pCO_2}\right)$$

In these formulas, pH_d is the desired pH, pH_c the current pH, and PKA the acid dissociation constant. A pH_d of 7.45 was aimed for before the kidney was connected to the NMP system, since the system was sensitive to acidification directly after the start of the kidney perfusion. During the rest of the NMP perfusion, the pH_d was 7.40. Glucose 5 % was added to aim for a minimal concentration of 5 mmol/L according to the formula:

$$\dots mL\ Glucose\ 5\ \% = (5 - [Glucose]) * 3.6 * V$$

In this formula, V is the total perfusate volume. Furthermore, the osmolarity of the perfusate was monitored, since electrolytes were excreted in the

urine and not recirculated. To estimate the osmolarity, the following formula was used:

$$Osmolarity = 2[Na^+] + 2[K^+] + [Glucose] + [Urea]$$

All concentrations in this formula are in mmol/L. The calculated osmolarity was be kept in a 275-295 mOsmol/kg range. An osmolarity lower than 275 mOsmol/L was corrected by adding 10x Hank's Balanced Salt Solution (HBSS) to the perfusate, according to the formula:

$$\dots mL\ 10x\ HBSS = (290 - Osmolarity) * 0.34 * V$$

This formula aims for a osmolarity of 290 mOsmol/kg.

After a maximum of 24 hours of HMP, the kidney was detached from the HMP system. An 8-10 Fr arterial cannula was placed in the ureter and fixated. Visceral fat surrounding the kidney was removed until there was a clear view on the kidney cortex. A punch biopsy was taken and the biopsy spot was sutured. The main branches of the arteria (a.) renalis were identified and a loop was placed around one of them to make later identification easier. The kidney was flushed with 200-500 mL Ringers lactate at 25-37 °C. The weight of the kidney was determined including the cannulas. The cannulas were filled with perfusate, the kidney was connected to the NMP system, and pressure controlled circulation at 75 mmHg was started. It was checked whether the colour of the kidney cortex changed from blank to red properly. Directly after the start of NMP, infusion of epoprostenol and Soluvit N (*table 1*) in aminoplasmal 10 % was started at 10 mL/h. Each kidney was perfused for 2 hours to obtain a steady-state. Urine was collected in a collection bin. During the steady-state perfusion, pH, glucose, and osmolarity were determined 5, 25, 45, 65, 85 and 105 min after the start of NMP. When these were aberrant, $NaHCO_3$, glucose 5 %, or 10x HBSS were infused to reach their target values as previously described.

After the steady-state phase, the intervention phases were started. At the end of the experiment, the kidney was disconnected from the NMP system. The kidney was weighed including the cannulas and a wedge biopsy was taken.

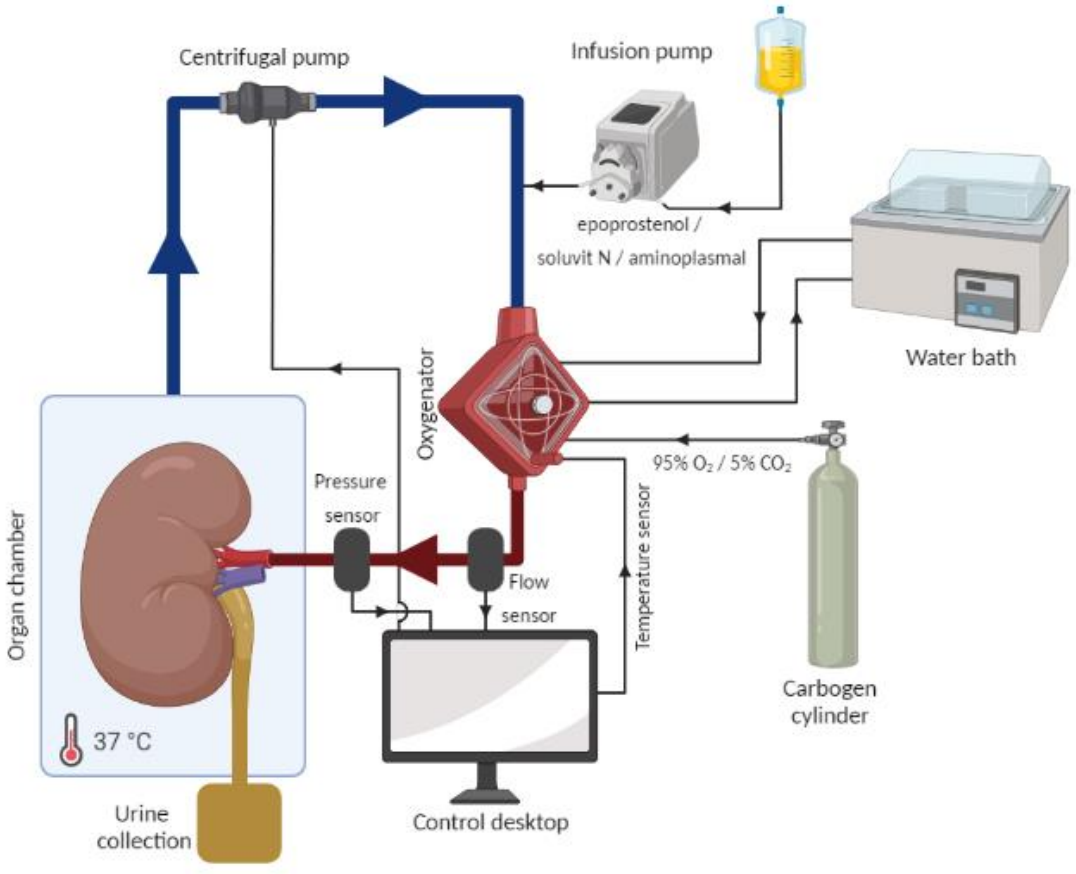

Figure 3
Schematic overview of the NMP system used for warm oxygenated preservation.

Table 1
Overview of the infusions during the kidney NMP.

Product	Dose	Infusion speed
Epoprostenol (Flolan)	0,08 mg in 8 mL Flolan solvent in 42 mL aminoplasmal 10%	10 ml/h
Soluvit N	1 vial in 50 mL aminoplasmal 10 %	

Interventions

The intervention phases consisted of stepwise pressure decrease and increase, and periods of arterial branch clamping and reperfusion. In the second successfully finished experiment for each optical method, the order of these phases was reversed.

Stepwise pressure decrease and increase

During this intervention phase, the pressure control was first decreased to 0 mmHg and then increased back to 75 mmHg in steps of 5 min each. The first three pressure decreases were 5 mmHg each. Hereafter, the pressure was decreased to 0 mmHg in three steps of 20 mmHg. In the second half of this phase, the pressure was increased to 75 mmHg in three steps of 20 mmHg followed by three steps of 5 mmHg.

Arterial branch clamping and reperfusion

To determine the degrees of differentiation for local differences in the microcirculation of each optical method, the blood circulation in the kidney was locally obstructed by clamping one of the main branches of the a. renalis. During this phase, the arterial branch that was identified before the start of NMP was clamped for 3 periods of 5, 10, and 15 min consecutively. Each clamping period was followed by a reperfusion period that was twice as long as this period.

Conventional functionality assessment

Besides measuring the pH, glucose level and osmolarity of the perfusate, biomarkers in the perfusate and produced urine that could indicate kidney functionality were measured. At set time points, arterial and venous perfusate, and urine samples were taken and analysed with a blood gas analyser. These time points and the biomarkers measured in each sample are listed in *tables 2* and *3* respectively. The arterial samples were taken directly from the arterial perfusate supply tube. To prevent errors in the venous measurements due to the blending of the perfusate, the venous samples were taken from the perfusate flowing out of the vena (v.) renalis. The urine samples were taken from the urine collection bucket. Moreover, the volume of the produced urine was noted and a new bucket was placed at the sample time points. Removed sample volume was corrected for in the volume measurements. During the stepwise pressure decrease and increase phase, the urine volume was noted every 5 min.

The oxygen consumption (VO_2) was calculated from the RBF, arterial and venous haemoglobin (Hb_a and Hb_v), arterial and venous oxygen saturation (S_aO_2 and S_vO_2), and arterial and venous partial oxygen pressure (p_aO_2 and p_vO_2) using the formulas (61):

$$VO_2 = RBF(C_aO_2 - C_vO_2)$$

$$Arterial\ oxygen\ content: C_aO_2 = (Hb_a \cdot 1.36 \cdot S_aO_2) + (0.0031 \cdot p_aO_2)$$

$$Venous\ oxygen\ content: C_vO_2 = (Hb_v \cdot 1.36 \cdot S_vO_2) + (0.0031 \cdot p_vO_2)$$

Moreover, creatinine clearance (Cl_{Cr}) was calculated from the perfusate and urine creatinine concentrations (Cr_p and Cr_u), and the urine volume (V_u) using the formula (61):

$$Cl_{Cr} = \frac{Cr_u \cdot V_u}{Cr_p}$$

Furthermore, the fractional sodium excretion (FE_{Na}) was calculated from the perfusate and urine sodium concentrations (Na_p and Na_u), and the perfusate and urine creatinine concentrations (Cr_p and Cr_u) using the formula (62):

$$FE_{Na} = \frac{Na_u \cdot Cr_p}{Na_p \cdot Cr_u} \cdot 100\%$$

Besides the perfusate biomarker analysis, histological analysis on the biopsies taken was performed. The biopsies were stored at room temperature on formaline for a minimum of 24 hours. Hereafter, they were washed with ethanol 70% and stored at 7 °C on ethanol 70%. The biopsies were embedded in paraffin wax and a microtome was used to cut slices. These slices were stained with a hematoxylin and eosin stain and scanned with a digital microscope.

Pictures of the kidneys were taken at all time points at which the urine volume was noted (*table 2*). These pictures were used to compare the results of the optical methods with the macroscopic appearance of the kidney. Lastly, the measured temperature, renal blood flow (RBF), and pressure were saved every second during the experiments. VO_2, Cl_{Cr}, urine production, and RBF were corrected for the average weight of the kidney.

Table 2
Overview of the time points at which biomarkers were measured during the experiment. * = every 5 min

	Time (min)	Samples			V_U	Photo
		Arterial	Venous	Urine		
Steady-state NMP	*-30*	✓				✓
	5	✓			✓	✓
	25	✓			✓	✓
	45	✓			✓	✓
	65	✓			✓	✓
	85	✓			✓	✓
	105	✓	✓	✓	✓	✓
	120				✓	✓
Pressure decrease-increase	*0-30**				✓	✓
	30	✓	✓	✓	✓	✓
	*30-60**				✓	✓
	60	✓	✓	✓	✓	✓
Arterial branch clamping	*5*	✓	✓	✓	✓	✓
	15	✓	✓	✓	✓	✓
	25	✓	✓	✓	✓	✓
	45	✓	✓	✓	✓	✓
	60	✓	✓	✓	✓	✓
	90	✓	✓	✓	✓	✓

Table 3
Overview of the measured biomarkers in the arterial, venous and urine samples during the experiment. * = calculated and not measured directly

Biomarker	Arterial	Venous	Urine
pH	✓	✓	
pO_2	✓	✓	
SO_2	✓*	✓*	
pCO_2	✓	✓	
Lactate	✓	✓	
Na^+	✓	✓	✓
K^+	✓	✓	✓
Glucose	✓	✓	✓
Urea	✓	✓	✓
Creatinine	✓	✓	✓
Hematocrit	✓	✓	✓
Haemoglobin	✓*	✓*	✓*

Optical imaging and measuring

Laser Speckle Contrast Imaging

The LSCI device (Pericam PSI NR, Perimed) was placed 27 cm above the kidney surface, which resulted in an imaged window of 16.2*13.6 cm. For the recordings, the frame rate was set at 2.1 images/s and the colour photo rate at 1 image/min. The image resolution was 0.20 mm/pixel. The recording was started before the kidney was connected to the NMP system and ended 10 min after the experiment was finished. Time points of manipulations to the positions of the LSCI device and the kidney were noted, since these cause artefacts.

Near Infrared Spectroscopy

The sensor stickers of the NIRS device (INVOS 7100, Medtronic) were placed in a sterile transparent ultrasound probe cover. Potential interference of the NI light with the cover was examined by placing a covered and a non-covered sensor sticker on a specific spot on a human forehead in changing orders. This experiment was repeated twice and none of the experiments showed a systematic difference in the signals derived from covered and non-covered sensor stickers. Therefore, it was assumed that potential interference caused by the cover did not have a relevant influence on the NIRS signal for the kidney NMP experiment.

The kidney was divided into quadrants and in each of the quadrants, one covered NIRS sensor was placed. To secure the position of the sensor, an elastic net was placed around the kidney. The sensors were placed on the anterior and posterior sides and their positions were crossed. The recording was started before the kidney was connected to the NMP system and ended 10 min after the experiment was finished.

Sidestream Dark Field Imaging

To position the SDFI device (MicroScan, MicroVision Medical), 4 clamps were placed that each positioned the probe tip in the centre of a kidney quadrant. At set time points, recordings with a length of 150 frames were made in all quadrants in the same order. During the steady-state NMP phase, the tissue was recorded every 10 min starting at 0 min and ending at 120 min after the start. An additional recording was made at 5 min. In the stepwise pressure decrease and increase phase, recordings were made every 2.5 min. During the arterial branch clamping and reperfusion phase, the tissue was recorded every 2.5 min in the 5 and 10 min periods and every 5 min in the 15, 20 and 30 min periods.

Analysis

Laser Speckle Contrast Imaging

The recordings created with LSCI were analysed using a data acquisition and analysis software program (PIMSoft, Perimed) designed to be used with the LSCI system. In this software, the means and standard deviations of the signal in specific timeframes and ROIs were calculated. The 95 % confidence intervals were calculated from the standard deviations. Timeframes of 20 s were set every 5 min during the steady-state NMP phase with 2 additional timeframes at 2.5 and 7.5 min after the start of NMP. During the stepwise pressure decrease and increase phase, timeframes were set every min. In the arterial branch clamping and reperfusion phase, timeframes were set every 1 min in the first 5 min of a period, every 2 min in the second 5 min and every 4 min in the resting time. Timeframes that contained manipulation artefacts were replaced with an artefact-free timeframe. When no artefact-free timeframe could be set within the 35 s before or after the intended starting point of the timeframe, the timeframe was removed.

In total, 5 ROIs were created in the images of the recordings. The first ROI contained the whole kidney cortex except for the outer 1-2 cm. Each of the other ROIs was placed in a kidney quadrant. These ROIs followed the same border as the first ROI on the outside. On the inside, straight borders were set parallel to the midlines of the kidney with a margin of 0.5 – 1.5 cm to each other. An example can be seen in *figure 4*.

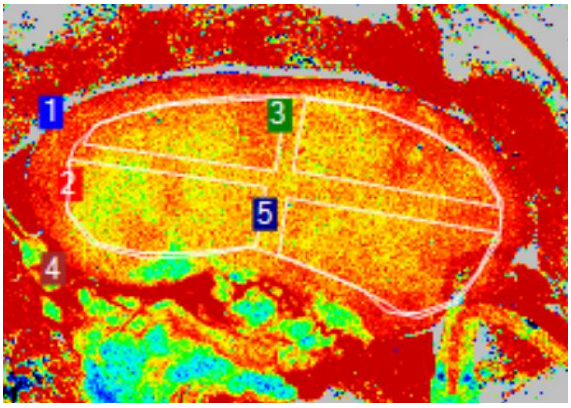

Figure 4
The ROIs for analysis of the LSCI recordings. ROI 1 contains the whole kidney and ROIs 2 – 5 each contain a quadrant.

Near Infrared Spectroscopy

The recordings created with NIRS were processed and converted to a CSV file using a data acquisition and analysis software program (Invos Analytics Tool, Medtronic) designed to be used with the NIRS system. Hereafter, the mean signal and standard deviations of every 5 min after the start of NMP were calculated. The 95 % confidence intervals were calculated from the standard deviations.

Sidestream Dark Field Imaging

The recordings created with SDFI were analysed using an analysis software program (AVA 4, MicroVision Medical) designed to be used with the SDFI system. The number of crossings, perfused number of crossings and proportion of perfused vessels (PPV) were calculated from each of the recordings by an algorithm specifically designed for the SDFI device used in the experiments.

Correlation analysis

For the methods that showed any response to the interventions in at least two different kidneys, correlations with the VO2, FENa, ClCr, urine production and RBF were analysed. For each time point at which VO2, FENa, ClCr, and urine production were analysed in the steady-state NMP and arterial branch clamping and reperfusion phases, the preceding averaged value of the measured signal was matched. Averaged signals in the stepwise pressure decrease and increase phase were matched with the averaged RBF over the preceding 20 s. Pearson's r with a 95 % confidence interval and two-tailed p-value was calculated for the individual kidneys and all kidneys combined. The correlation coefficient was considered significant when $p < 0.05$.

Comprehension of the optical methods

To acquire equal comprehension of LSCI, NIRS and SDFI, the methods were scored on a list of (semi-)objective metrics (*table 4*). These metrics represented characteristics that were expected to be relevant to methods used in clinical practice. The list and the order of importance were created in cooperation with transplant surgeons and a technical physician who were experienced in kidney NMP. *Reproducibility* was assessed in the steady-state NMP phase, *differentiation* in the arterial branch clamping and reperfusion phase, and *sensitivity* in the stepwise pressure decrease and increase phase.

Table 4

Descriptions and examples of the metrics used to achieve equal comprehension of the methods. The order represents the importance of the metrics. The most important metrics are on top.

Metric	Description	Rationale
Sterility	The risk of introducing pathogens to the kidney surface when using the optical method, while optimal precautions are present.	High risk of introducing pathogens to the kidney surface impedes the implementation in clinical practice.
Reproducibility	The amount of variation in the measured signals under the assumption that the circumstances did not change.	Low reproducibility makes it harder to compare inter- and intra-individual results.
Differentiation	The ability of a method to show spatial differences in perfusion.	Vessel occlusions can cause local differences in perfusion and imaging or measuring the size of the affected area could help in considering treatment.
Velocity	The fraction of the kidney that can be measured within 1 min.	Low velocity limits the reliability since affected areas could be missed in a kidney when the perfusion is not equally divided over the kidney.
Sensitivity	The amount of pressure change to which the measured signal shows a response.	Unstable signals have limited sensitivity, which is disadvantageous to functionality assessments.
Preparation	The time and effort needed to set up the device for 1 employee.	Time and effort-consuming preparation could be disadvantageous to the implementation in clinical practice.
Workload	The effort needed to image or measure.	High workload could be disadvantageous to the implementation in clinical practice.
Interpretation	The effort needed to interpret the images or measurements.	Difficult interpretation could be disadvantageous to the implementation in clinical practice.
Invasiveness	The interaction with the kidney needed to image or measure.	Invasive interaction with the kidney could harm the kidney and threaten transplantation.
Spatial resolution	The size of the kidney surface an image pixel or measured signal represents.	Low spatial resolutions limit reliability.
Temporal resolution	The sampling frequency in which images or measurements are created.	Low temporal resolutions limit reliability.
Window	The fraction of the kidney surface that could be imaged or measured simultaneously.	Reliability is reduced for methods that can not image the whole kidney simultaneously in real-time.
Usability	The amount of skills needed to acquire usable images or measurements.	Large learning curves could be disadvantageous to the implementation in clinical practice.
Costs (device)	The costs of the imaging or measuring device.	High costs of the device could be disadvantageous to the implementation in clinical practice.

Table continues on the next page

Table 4 (continuation)

Metric	Description	Rationale
Costs (additional items)	The costs of additional items per experiment needed to image or measure one kidney.	High costs of the additional items could be disadvantageous to the implementation in the clinical practice.
Environment	The sensitivity to ambient electromagnetic radiation.	High sensitivity to ambient electromagnetic radiation requires covering up the kidney which limits the view on the kidney.
Depth	The maximal depth at which can be imaged or measured in theory.	Small depths limit the reliability since affected areas could be missed in a kidney when the perfusion is not equally divided over the kidney.

Table 5

Distribution of the scores for the (semi-)objective metrics. The order represents the importance of the metrics. The most important metrics are on top.

Metric	-	+/-	+
Sterility	High risk	Low risk	Almost no risk
Reproducibility	> 20 %	> 5 % ≤ 20 %	≤ 5 %
Differentiation	Spatial differences not detected	Spatial differences detected, but not consistent	Spatial differences consistently detected
Velocity	< 25 %	≥ 25 % < 50 %	≥ 50 %
Sensitivity	Flow changes after pressure changes not detected	Flow changes after a 20 mmHg pressure change detected	Flow changes after 5 and 20 mmHg pressure changes detected
Preparation	> 30 min	> 15 min ≤ 30 min	≤ 15 min
Workload	Additional manpower is required	Images or measurements can be created by currently available manpower	No manpower required at all
Interpretation	Results have to be analysed before they can be interpreted	Results can be interpreted directly, but this takes some effort	Results are clear and can be interpreted directly
Invasiveness	Pressure to the tissue required	Tissue contact required, but no pressure applied	No tissue contact required
Spatial resolution	> 1 mm/pixel	> 0.1 mm/pixel ≤ 1 mm/pixel	≤ 0.1 mm/pixel
Temporal resolution	< 1 Hz	≥ 1 Hz < 10 Hz	≥ 10 Hz
Window	< 20 %	≥ 20 % < 50 %	≥ 50 %
Usability	> 1 hour of training is needed to use the method	≤ 1 hour of training is needed to use the method	The method can be used without any training.
Costs (device)	> € 75 000,-	> € 25 000,- ≤ € 75 000,-	≤ € 25 000,-
Costs (additional items)	> € 10,-	> € 0,- ≤ € 10,-	€ 0,-
Environment	Sensitivity to electromagnetic radiation not solved by covering up	Sensitivity to electromagnetic radiation solved by covering up	Not sensitive to electromagnetic radiation
Depth	< 1 mm	≥ 1 mm < 10 mm	≥ 10 mm

Results

A total of 8 kidney NMP experiments were started of which 3 failed before the intervention phases were started. The reasons the experiments failed were assigned to micro thrombosis of the perfusate, a defective oxygenator and decreased kidney viability because of large HMP and post-HMP cold ischemia times. The kidneys, their characteristics, and ischemia and perfusion times are listed in *table 6*.

Table 6

Overview of the locations of the slaughterhouses of retrieval, order of the experiments, sides of the kidneys, warm ischemia times (WIT), cold ischemia times pre HMP (CIT_{pr}), HMP times (HMPT), cold ischemia times post HMP (CIT_{po}), NMP times (NMPT), weight pre-NMP (W_{pr}) and weight post-NMP (W_{po}). Times are in min. Weights are in grams. Unkn = unknown

Device	Kidney	Slaughterhouse	Order	Side	WIT	CIT_{pr}	HMPT	CIT_{po}	NMPT	W_{pr}	W_{po}
LSCI	1	Zevenaar	3	left	40	5	175	66	270	300	354
	2	Reeuwijk	4	right	35	10	135	58	285	330	381
	3	Reeuwijk	2	unkn	30	15	165	29	91	289	unkn
NIRS	1	Zevenaar	5	left	45	5	190	69	270	290	356
	2	Zevenaar	6	left	40	147	1140	58	270	459	460
	3	Zevenaar	1	unkn	35	40	252	89	34	unkn	unkn
SDFI	1	Zevenaar	8	right	45	140	1320	49	292	395	405
	2	Reeuwijk	7	left	30	16	1534	154	120	unkn	408

Laser Speckle Contrast Imaging

In total, 3 experiments with LSCI were started of which 2 were successfully ended. Results of the analysis of these LSCI recordings can be seen in *figure 5*. LSCI images and matching colour photos of specific points in time are shown in *figure 6*. In kidney 1, the arterial branch clamping and reperfusion phase was started first after the steady-state NMP phase. Kidney 2 was treated in the reversed order. Although treated the same, the LSCI signals responded differently to the start of NMP. The signal magnitudes and the degrees of differentiation between the regional LSCI signals were different. However, a 20 – 30 min phase after the start of NMP in which the signals reached their maximums was observed in both experiments. During this period, the RBF of kidney 2 remained stable at 125 – 135 mL/min. In kidney 1, the RBF data were not saved correctly.

The LSCI signal responses to the stepwise pressure decrease and increase interventions were different in the studied kidneys. Changes in the LSCI signal after a 5 mmHg decrease or increase in pressure were not significant, while significant changes were seen for steps of 20 mmHg. In kidney 1, a stepwise decrease and increase in LSCI signal were observed that responded in parallel to the pressure changes. However, in kidney 2, the signal dropped to a minimum when the pressure was decreased from 40 mmHg to 20 mmHg and did not change during the rest of this phase except for a small peak at 32 min after the start caused by sampling from the arterial tubing. Phenomena observed in both kidneys were short hypoperfusion periods directly after pressure decreases and short hyperperfusion periods directly after pressure increases. The morphology of these periods is illustrated in *figures 7A and 7B*.

Opposite responses to arterial branch clamping and releasing were observed in the 2 successfully perfused kidneys. In general, the signal increased during the clamping periods and decreased during the reperfusion periods in kidney 1. While this effect was clearly observed in the lateral ROIs, the effects in the medial ROIs were more subtle. In kidney 2, the signal decreased during the clamping periods and increased during the reperfusion periods in the caudal ROIs. The cranial medial ROI remained more or less stable during this phase, while the cranial lateral ROI was stable in the first 35 min and decreased slightly in the rest of this phase. During the 10 and 20 min reperfusion periods, reperfusion was not observed in the part of the kidney that was affected by clamping the arterial branch in the preceding period. Therefore, the infusion speed of the epoprostenol/Soluvit N solution was set at 30 mL/h for 1 min halfway the reperfusion period. Hereafter, a signal increase in the caudal ROIs was observed. Periods of hyperperfusion were observed in the ROIs in which the signal decreased during the clamping periods. An example is shown in *figure 7C*.

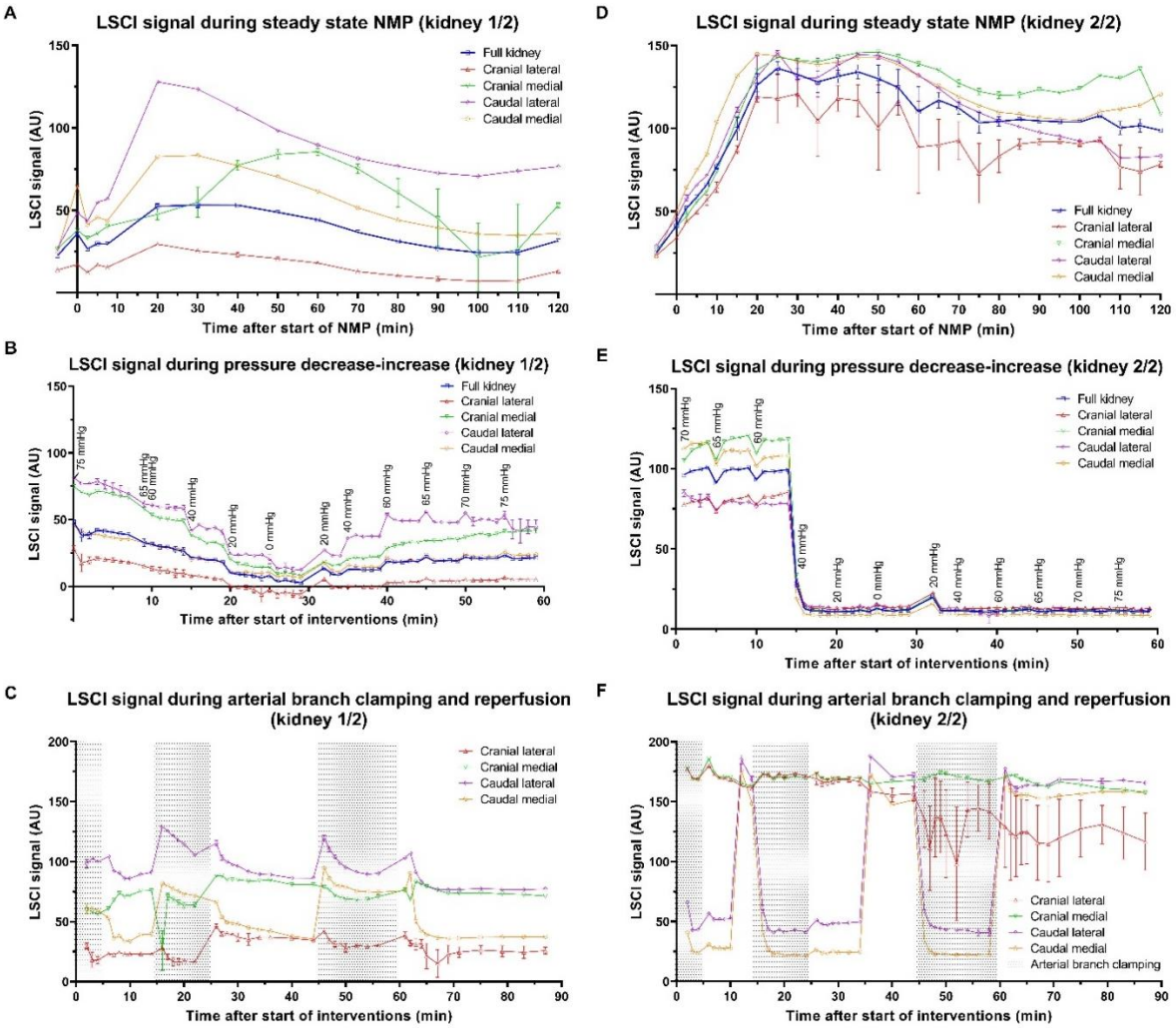

Figure 5

The LSCI signals and their 95 % confidence intervals during the steady-state NMP (A and D), stepwise pressure decrease and increase (B and E) and arterial branch clamping and reperfusion (C and F) phases.

Near Infrared Spectroscopy

In total, 3 experiments with NIRS were started from which 2 were successfully ended. Results of the analysis of these NIRS recordings can be seen in *figure 8*. In kidney 1, the arterial branch clamping and reperfusion phase was started first after the steady-state NMP phase. Kidney 2 was treated in the reversed order. In some of the timeframes used for signal averaging, no signal was detected. Therefore, there were some gaps in the analysed data. The NIRS signal of kidney 1 showed less variance in the steady-state NMP phase compared to kidney 2. Moreover, a 20-30 min phase after the start of NMP in which the signals reached a stable equilibrium was observed in kidney 1 and not in kidney 2.

In the stepwise pressure decrease and increase phase, the NIRS signals of the caudal and cranial lateral sensors of kidney 1 remained stable, while the cranial medial sensor showed variance over time that could not be properly related to the pressure changes. Moreover, the initial magnitude of the signal of this sensor was larger compared to the other sensors, which could be attributed to an increase in the signal of the preceding arterial branch clamping and reperfusion phase. In kidney 2, an increase in the signals was observed in all sensors during the period in which the pressure was decreased and vice versa. No significant signal changes were observed for the 5 mmHg steps.

In kidney 1, the NIRS signals remained stable during the arterial branch clamping and reperfusion phase. Only the signal of the cranial medial sensor showed an increase at the start of the 15 min clamping period, whereafter the signal remained stable with a slightly larger magnitude compared to the sensors in the other quadrants. In kidney 2, signals from some quadrants responded to the clamping and reperfusion periods by an increase and decrease respectively. However, the signals from the caudal quadrants did show this response in the first and second clamping and reperfusion periods, but not in the 15 min clamping period.

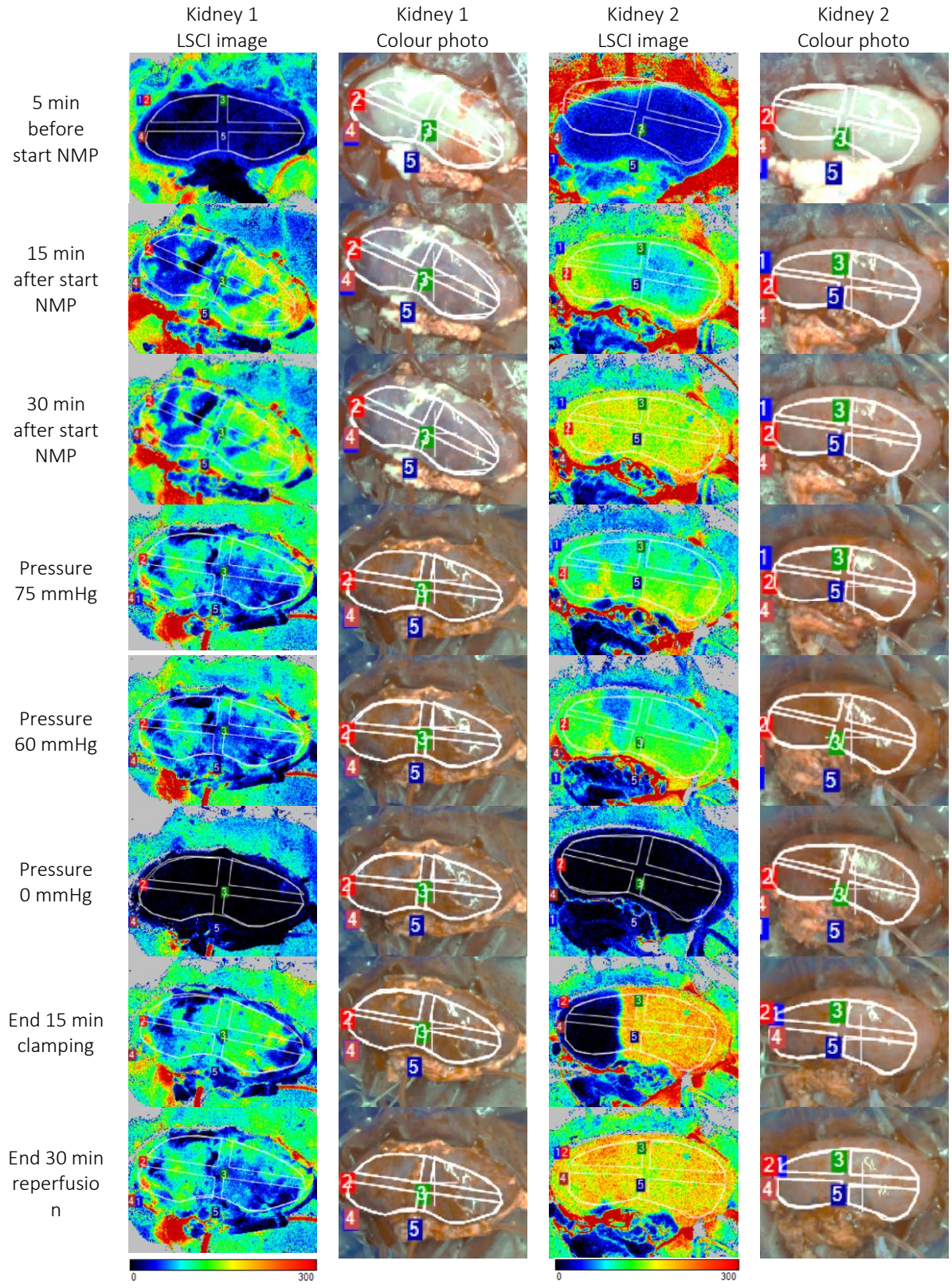

Figure 6

LSCI images and matching colour photos of some specific points in time. The examples from the stepwise pressure decrease and increase phase are from the decrease period. The ROIs on the colour photos do not match the actual positions of the ROIs.

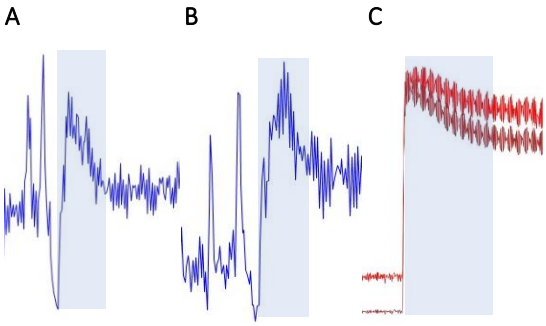

Figure 7

Morphology of the raw LSCI signals during periods of hyperperfusion after a 5 mmHg (A) and a 20 mmHg (B) increase in pressure, and after the release of an arterial branch clamp (C). The signals in images A and B represent the whole kidney, and the signals in image C are the ROIs in which the signal decreased during clamping. Hyperperfusion periods are marked.

Sidestream Dark Field Imaging

In total, 2 experiments with SDFI were started from which 1 was successfully ended. Since the recordings created with the SDFI device were blurred (*figure 9*) and did not contain relevant data, it was decided not to aim for a second successful experiment. Results of the analysis of the SDFI recordings can be seen in *figures 10 and 11*. Increasing numbers of crossings, perfused numbers of crossings and PPVs over time were calculated from the recordings for the steady-state NMP phase. In the intervention phases, no coherence between the interventions and the calculated numbers of crossings, perfused numbers of crossings and PPVs was observed.

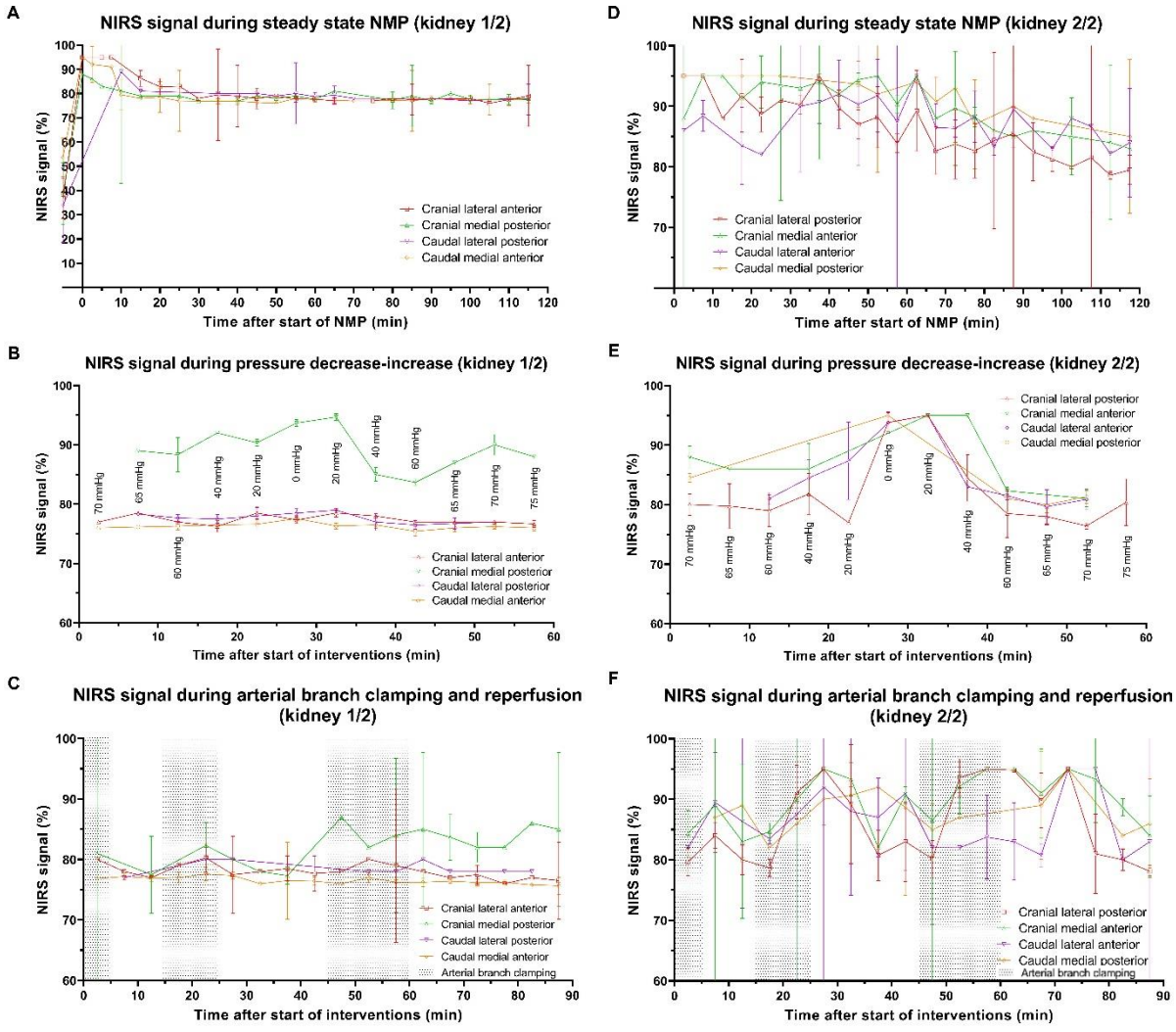

Figure 8

The NIRS signals and their 95 % confidence intervals during the steady-state NMP (A and D), stepwise pressure decrease and increase (B and E) and arterial branch clamping and reperfusion (C and F) phases.

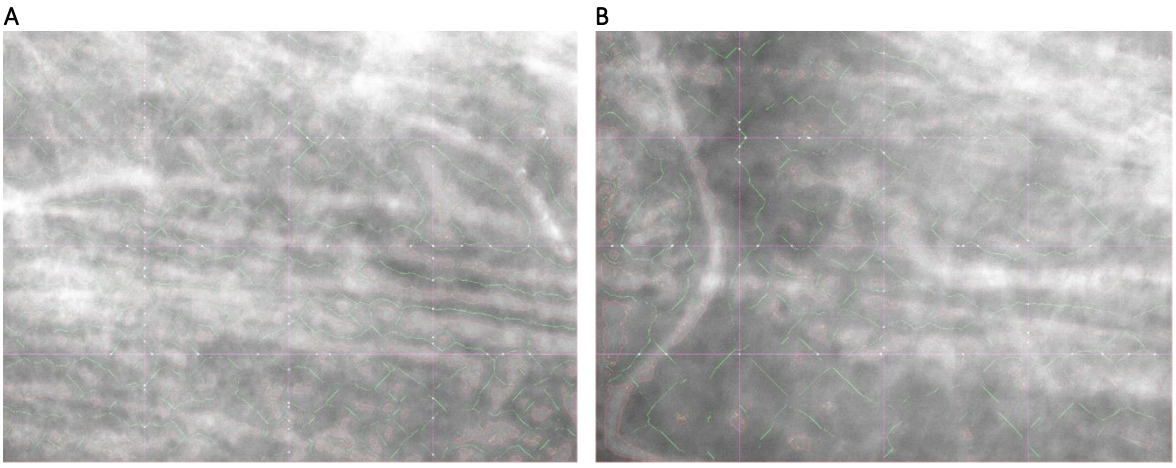

Figure 9

Shots of the analysed SDFI recordings at the end of the 15 min arterial branch clamping period (A) and the end of the 30 min reperfusion periods (B).

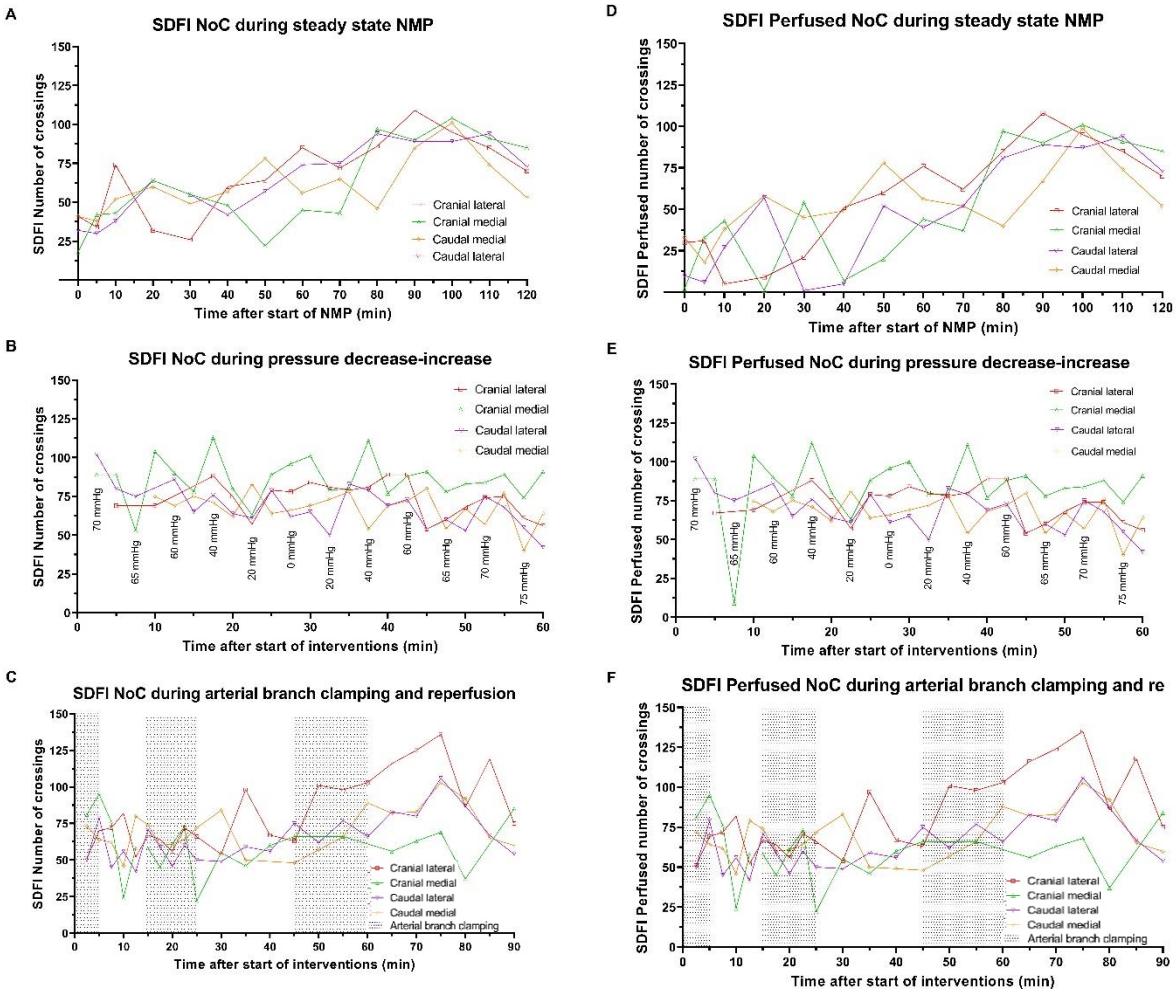

Figure 10

The number of crossings (NoC) (A – C) and perfused NoC (D – F) calculated from the SDFI recordings acquired during the steady-state NMP (A and D), stepwise pressure decrease and increase (B and E) and arterial branch clamping and reperfusion (C and F) phases.

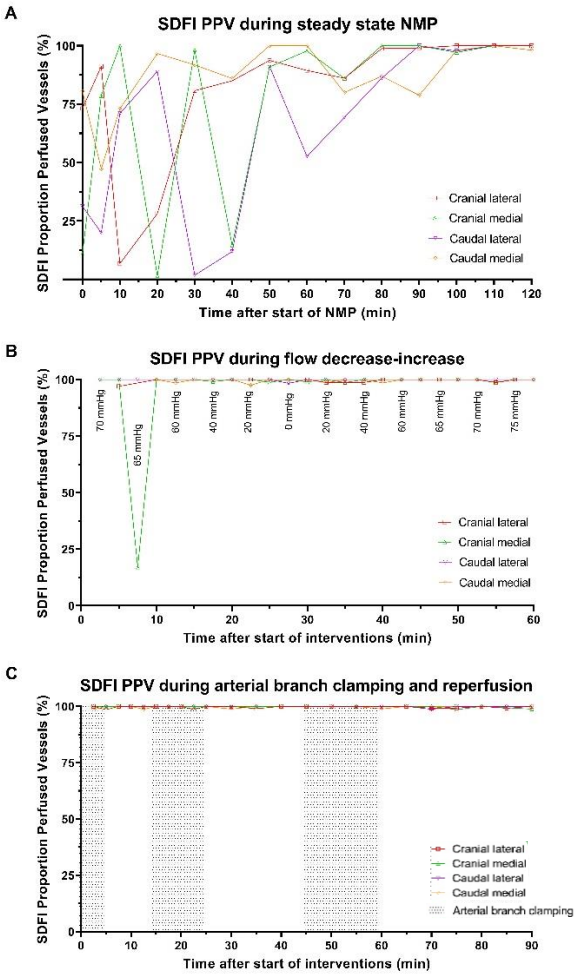

Figure 11
The PPV calculated from the SDFI recordings acquired during the steady-state NMP (A), stepwise pressure decrease and increase (B) and arterial branch clamping and reperfusion (C) phases.

Correlation analysis

Scatter plots of LSCI signals and matching VO_2, FE_{Na}, Cl_{Cr}, urine production, and RBF are shown in *figure 12*. The RBF was not correctly saved for kidney 1 and thus the VO_2 could not be calculated. Pearson's r values with 95 % confidence intervals and p-values for each kidney and the combined dataset are listed in *table 7*. Significant correlations were found between the LSCI signal and the VO_2 in kidney 2, the FE_{Na} in the combined dataset, the Cl_{Cr} in kidney 1, the urine production in the combined dataset, and the RBF in kidney 2.

Comprehension of the methods

Scores of the (semi-)objective metrics for the optical methods (*table 8*) were based on the results of the experiments and the characteristics of the methods. The costs of the LSCI and SDFI devices were based on the price paid for the purchase of the device and the additional items by the owner. For the NIRS device, these costs were based on a quote for the device received from the manufacturer. Since the depth at which was measured in the kidney tissue was not examined during the experiments, the assessment was based on the results of the literature study that preceded this research.

Histology

The biopsies taken before the start and after the end of NMP were assessed in general. In *figure 13,* sections of the biopsies of NIRS kidney 1 can be seen. No major deterioration was observed in the histological assessment. No notable damage to the glomeruli was observed under the microscope.

Table 7
The Pearson's r calculated between the LSCI signal and 5 conventional functionality assessments and their two-tailed P-values. CI = confidence interval, N = number of sets of variables, * = 95 % confidence interval not calculated because of small N

	Kidney	Pearson's r	95% CI	N	P-value
Oxygen consumption	2	0.79	0.20 – 0.96	8	0.019
Fractional Na^+ excretion	1	-0.01	-0.76 – 0.75	7	0.980
	2	0.95	*	3	0.201
	Both	-0.76	-0.94 - -0.24	10	0.011
Creatinine clearance	1	-0.82	-0.97 – -0.18	7	0.024
	2	-0.89	*	3	0.297
	Both	-0.25	-0.76 – 0.45	10	0.491
Urine production	1	-0.08	-0.63 – 0.52	12	0.798
	2	-0.05	-0.58 – 0.52	13	0.872
	Both	0.97	0.93 - 0.99	25	<0.001
Renal blood flow	2	0.87	0.79 – 0.92	57	<0.001

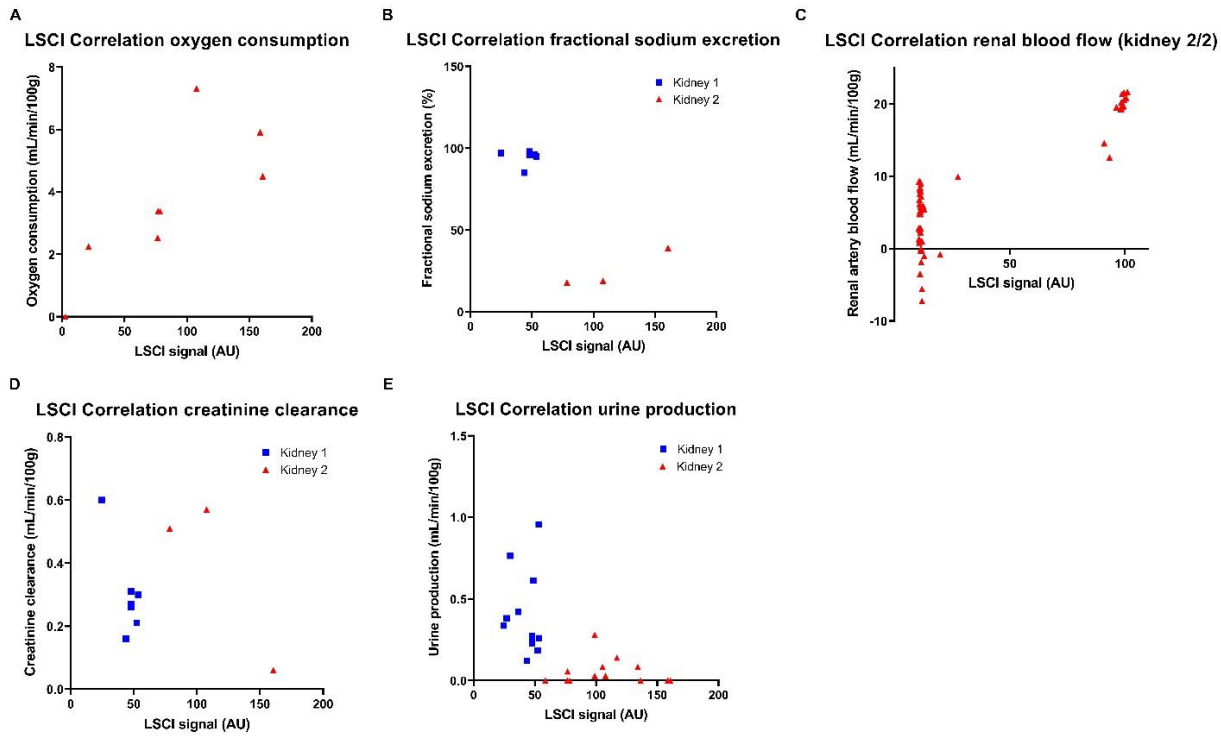

Figure 12

Scatter plots of the LSCI signal and matching VO_2 (A), FE_{Na} (B), RBF (C), Cl_{Cr} (D) and urine production (E) for both kidneys.

Table 8

Scores of each of the (semi-)objective metrics for the optical methods. The order represents the importance of the metrics. The most important metrics are on top.

Metric	LSCI	NIRS	SDFI
Sterility	+	+/-	+/-
Reproducibility	+/-	**+/-**	-
Differentiation	+	+/-	-
Velocity	+	-	-
Sensitivity	+/-	+/-	-
Preparation	+/-	+/-	+
Workload	+/-	+	-
Interpretation	+	+/-	-
Invasiveness	+	+/-	+/-
Spatial resolution	+/-	-	**+**
Temporal resolution	+	+	**+**
Window	+	-	-
Usability	+/-	+	+/-
Costs (device)	+/-	+	**+/-**
Costs (additional items)	+	-	**+/-**
Environment	+	+/-	+
Depth	+/-	+	-

Discussion

This study aimed to compare the use of LSCI, NIRS and SDFM for quantification of organ microcirculation, during kidney NMP. In total, 8 porcine slaughterhouse kidney NMP experiments were started from which 5 successfully ended. The results showed the response of the optical methods to steady-state NMP, a stepwise pressure decrease and increase, and clamping and releasing of an arterial branch. From comprehension of the methods by (semi-)objective metrics, it can be concluded that LSCI is the most promising method for further development towards a clinical objective transplantability assessment tool. This supports the conclusion of the literature review with a more objective assessment underlying.

The results of this study contributed to the existing knowledge about the use of optical imaging and measuring methods for the quantification of organ microcirculation during periods of ischemia and reperfusion. The knowledge about the methods used in this study was limited to studies in rodents (63, 64) and pigs (55). Since the size and physiology of porcine and human organs are closer related than rodent and human organs, the knowledge from studies in rodents was considered less relevant. A study by *Heeman et al.* that combined the use of LSCI and SDFI on porcine slaughterhouse kidneys during

NMP is considered the most closely related to this study (55). Experiments in other studies differed significantly from this study and were therefore not considered.

Heeman et al. showed that LSCI can identify a stepwise decreased blood flow in a similar experiment as in this study. They reduced the RBF in 4 steps of 50 mL/min from 200 mL/min to 0 mL/min. Since the degree of differentiation of the optical methods had to be unravelled in this study, it was chosen to reduce the flow in much smaller steps. This helped to identify the differences between the optical methods. In kidney 1, a similar response pattern of the LSCI signal was found as the pattern found in the study by *Heeman et al*. However, kidney 2 showed a sudden decrease in LSCI signal when the pressure was decreased to 40 mmHg which was probably more related to the kidney physiology than to the measurements.

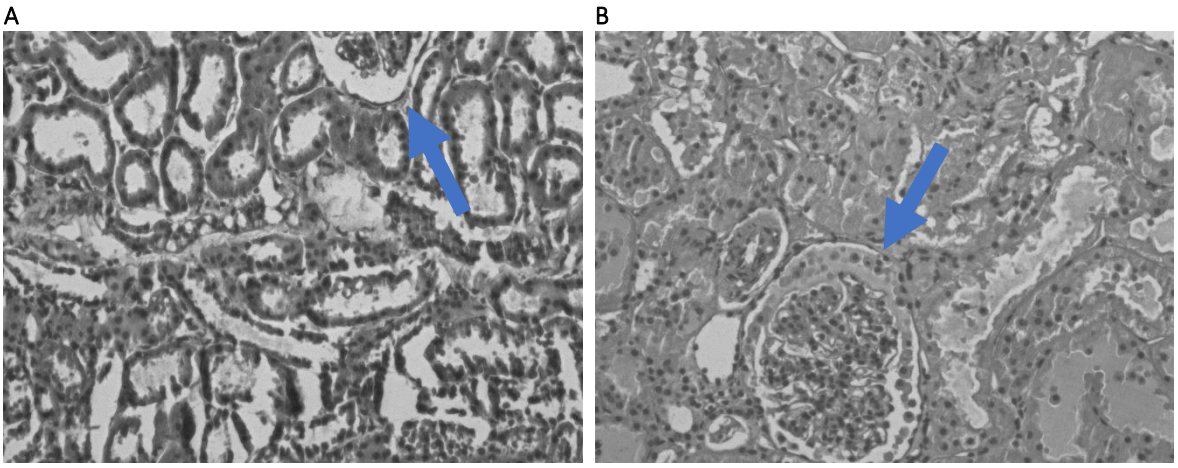

Figure 13
Microscopic sections of a punch biopsy before the start of NMP (A) and a wedge biopsy after the end of NMP (B). In each of the sections, glomeruli are indicated by an arrow.

Furthermore, the use of SDFI to assess organ microcirculation was examined in the study by *Heeman et al*. In this study, the renal capsule was locally removed, which rejects this protocol for clinical practice. Since they did not report on the limitations of imaging through the renal capsule, these were examined in this study. All recordings created with SDFI in 2 experiments were blurred, which could have been caused by a light disturbance in the capsule. This confirms the statements of *Heeman et al.* and it can be concluded that SDFI cannot be used in clinical practice for imaging of the kidney cortex.

No studies in which NIRS was used as a method to assess microcirculation of organs were published before. Therefore, it was unknown whether the NIRS sensors can measure the StO_2 in kidneys. It can be concluded that the sensors can detect signals from the tissue. However, the signal was extremely unstable and the temporal resolution was limited to 0.009 Hz. Therefore, the advantages of the real-time signals that are detected in cerebral and leg measurements are limited in kidneys. Although the signal was unstable, the reliability of this method was not unpromising. A trend can be observed in the response to the interventions, although this was not as consistent as in the LSCI experiments. This suggests that NIRS can be considered as a method to quantify organ microcirculation if the technological limitations could be solved.

In general, optical methods that image or measure microcirculation have shown their potential contribution to the assessment of organ functionality in kidneys. Some significant correlations between the LSCI signal and conventional functionality assessments were found. However, the numbers of samples and numbers of kidneys on which this correlation was based were small and the correlations were only significant in one kidney or the combined dataset. Therefore, these significant correlations could not be considered clinically relevant. Moreover, the relevances of the 5 functionality assessments that were considered in this study are questionable. Although these have been used in other studies to assess the functionality of kidneys during NMP, no relation with the outcome after transplantation has been demonstrated (61, 62). Lastly, the variables of the 2 kidneys that were assessed were clustered at different locations in *figure 12*, which indicates that the comprehension between the kidneys is limited.

This confirms the observation that the individual kidneys showed different appearances during the experiments. A larger dataset with larger numbers of samples and included kidneys is needed to show whether there is a clinically relevant correlation between the LSCI signal and the conventional functionality assessments.

Although the anatomy, physiology and histology of other organs than the kidney differ, it is assumed that the results of this study show the potential of imaging or measuring the microcirculation in organs with a metabolic function and similar cell density. It is expected that the tissue of organs such as the liver, pancreas, and spleen react similarly to the emitted light. However, in organs that are more divergent, such as the heart and the bone structures, the reaction to light can be different. Therefore, the results of this study are probably less relevant to these organs.

Limitations

Logistic limitations resulted in the need to maintain the kidney on the HMP device overnight. Therefore, the blood and kidney had to be preserved for 20 – 24 hours. Bias could have been caused by different HMP treatment times of the first 5 kidneys and the other kidneys. Kidney preservation on HMP for 24 hours was studied by *Venema et al.* and was found to be advantageous when compared to SCS and non-oxygenated machine perfusion (65). Moreover, their results suggested that a subsequent NMP period of at least 4 hours can be successful. The quality of the blood after different preservation methods was examined in a short experiment before the first NMP experiment was performed with kidneys preserved for > 4 hours. The preservation on a CPG buffer that contained less glucose compared to the buffer used in the blood preservation experiment was successful and after pH correction, the NMP experiments proceeded uncomplicated. Therefore, the bias caused by this limitation is considered negligible.

In this study, the duration of the arterial branch clamping and reperfusion periods was increased in three steps. This stepwise increase in the duration of the occlusion and reperfusion periods has been executed before by *Heeman et al.* They demonstrated that RBF and LSCI signals recover within 10 min after a 5 min period of occlusion and within 40 min after a 15 min period. Therefore, it was assumed that the chosen lengths of the reperfusion periods were enough for the affected areas to recover. The results of the LSCI measurements in this study reported similar recovery times, although the affected areas in kidney 2 did not recover within the first half of the reperfusion period, which was treated with an epoprostenol bolus. This treatment was applied to prevent failure of the perfusion in a later stadium of the experiment. However, by adding a bolus of epoprostenol to the treatment, this kidney was treated differently than the other kidneys. It remains unknown whether the kidney would have recovered by itself when no bolus was added. Although this can be considered a limitation, the effect on the objective assessment of the optical methods is expected to be limited.

In this study, optical methods that provide information about microcirculation were assessed. However, in the literature review, methods that assess mitochondrial metabolism, such as flow-mediated skin fluorescence (FMSF), were considered besides these. Measuring mitochondrial metabolism could predict post-implantation organ functionality since efficient production of energy in the mitochondria depends on the delivery of nutrients and oxygen which is impaired during ischemic periods (66). Therefore, mitochondrial metabolism measurements could add value to the current functionality assessment of organs during NMP. In this study, methods that measure mitochondrial metabolism were not available for the experiments. Since the relevance of these methods for the functionality assessments of organs is considered high, it is suggested that these must be examined soon.

The added value of the analysis of the perfusate samples and biopsies taken in the experiments to the results and conclusions was kept limited in this study. Relations between the perfusate samples and the measured signals were exclusively performed for methods that showed response to the interventions in at least 2 kidneys. Analysis of the samples for methods that showed less response was expected to be irrelevant since the results could be biased by coincidental findings. Moreover, no control group was included, which limits the relevance of perfusate and biopsy analysis even more. Therefore, nothing could be concluded from the correlation and histology analyses. In continuation of this study, an experiment should be designed in which a control group is included and higher numbers of kidneys and samples are taken. Only then it could be justified to conclude that a significant correlation is clinically relevant. Since the evidential value of a certain experiment can be large, it would be useful to compare the signals of an optical method with the NMP assessment score that was published by *Hosgood et al.* and still remains the only validated kidney functionality assessment during NMP (29). The LSCI results in this study show the potential of this method and support proceeding with such experiments.

Acknowledgements

During this master thesis research, a bunch of medical professionals and technicians helped to achieve the purpose of this study. First, I am grateful for the input from everyone involved in the LUMC machine perfusion research group regarding the literature review and the design of the experiment. In particular, I would like to thank M.J.A. de Haan BSc., A.S. Arykbaeva BSc., and E. Gommers BSc. for their help during the execution of the experiments. Moreover, I would like to thank Ing. E.H. van Rossenberg and Drs. A.M.A. de Graaf for their help in retrieving the kidneys at the slaughterhouses and the transport to the LUMC. In the last place, I would like to thank my medical supervisors Prof. Dr. I.P.J. Alwayn, Dr. V.A.L. Huurman and Dr. D.K. de Vries, and my technical supervisor Dr. J.B. Doppenberg for their input and support during the design, execution, and analysis of the experiments.

References

1. Aaronson PIW, J. P. T.; Connolly, M. J. The Cardiovascular System at a Glance. 4 ed: John Wiley & Sons; 2013.
2. Anglicheau D, Tinel C, Canaud G, Loupy A, Zuber J, Delville M, et al. [Renal transplantation: Procedure and early follow-up]. Nephrol Ther. 2019;15(6):469-84.
3. Homer-Vanniasinkam S, Crinnion JN, Gough MJ. Post-ischaemic organ dysfunction: a review. Eur J Vasc Endovasc Surg. 1997;14(3):195-203.
4. Granger DN. Role of xanthine oxidase and granulocytes in ischemia-reperfusion injury. Am J Physiol. 1988;255(6 Pt 2):H1269-75.
5. Chambers DE, Parks DA, Patterson G, Roy R, McCord JM, Yoshida S, et al. Xanthine oxidase as a source of free radical damage in myocardial ischemia. J Mol Cell Cardiol. 1985;17(2):145-52.
6. McCully JD, Wakiyama H, Hsieh YJ, Jones M, Levitsky S. Differential contribution of necrosis and apoptosis in myocardial ischemia-reperfusion injury. Am J Physiol Heart Circ Physiol. 2004;286(5):H1923-35.
7. Seal JB, Gewertz BL. Vascular dysfunction in ischemia-reperfusion injury. Ann Vasc Surg. 2005;19(4):572-84.
8. Hill JH, Ward PA. The phlogistic role of C3 leukotactic fragments in myocardial infarcts of rats. J Exp Med. 1971;133(4):885-900.
9. Dorweiler B, Pruefer D, Andrasi TB, Maksan SM, Schmiedt W, Neufang A, et al. Ischemia-Reperfusion Injury : Pathophysiology and Clinical Implications. Eur J Trauma Emerg Surg. 2007;33(6):600-12.
10. Lumsden CJ, Silverman M, Zielinski A, Potts DG, Shafik I, Brody AS, et al. Vascular exchange in the kidney. Regional characterization by multiple indicator tomography. Circ Res. 1993;72(6):1172-80.
11. Flores J, DiBona DR, Beck CH, Leaf A. The role of cell swelling in ischemic renal damage and the protective effect of hypertonic solute. J Clin Invest. 1972;51(1):118-26.
12. Angelescu M, Kraus T, Wiesel M, Hergesell O, Haberkorn U, Klar E. Assessment of renal graft function by perioperative monitoring of cortical microcirculation in kidney transplantation. Transplantation. 2003;75(8):1190-6.
13. Wang HK, Chou YH, Yang AH, Chiou SY, Chiou HJ, Wu TH, et al. Evaluation of cortical perfusion in renal transplants: application of quantified power Doppler ultrasonography. Transplant Proc. 2008;40(7):2330-2.
14. Benz S, Bergt S, Obermaier R, Wiessner R, Pfeffer F, Schareck W, et al. Impairment of microcirculation in the early reperfusion period predicts the degree of graft pancreatitis in clinical pancreas transplantation. Transplantation. 2001;71(6):759-63.
15. Seifalian AM, Mallet SV, Rolles K, Davidson BR. Hepatic microcirculation during human orthotopic liver transplantation. Br J Surg. 1997;84(10):1391-5.
16. Connolly JK, Dyer PA, Martin S, Parrott NR, Pearson RC, Johnson RW. Importance of minimizing HLA-DR mismatch and cold preservation time in cadaveric renal transplantation. Transplantation. 1996;61(5):709-14.

17. Scheeren TW, Martin K, Maruschke M, Hakenberg OW. Prognostic value of intraoperative renal tissue oxygenation measurement on early renal transplant function. Transpl Int. 2011;24(7):687-96.
18. Drezza JPdO, Boteon APCdS, Calil IL, Anna RSS, Viveiros MdM, Rezende MBd, et al. Disposal of donor livers in Brazil: how to optimize their utilization rate in transplants? Einstein (Sao Paulo). 2021;19:eAO6770-eAO.
19. Tatum R, O'Malley TJ, Bodzin AS, Tchantchaleishvili V. Machine perfusion of donor organs for transplantation. Artif Organs. 2021;45(7):682-95.
20. Weissenbacher A, Vrakas G, Nasralla D, Ceresa CDL. The future of organ perfusion and re-conditioning. Transpl Int. 2019;32(6):586-97.
21. van Smaalen TC, Hoogland ER, van Heurn LW. Machine perfusion viability testing. Curr Opin Organ Transplant. 2013;18(2):168-73.
22. Muller X, Schlegel A, Kron P, Eshmuminov D, Würdinger M, Meierhofer D, et al. Novel Real-time Prediction of Liver Graft Function During Hypothermic Oxygenated Machine Perfusion Before Liver Transplantation. Ann Surg. 2019;270(5):783-90.
23. Guzzi F, Knight SR, Ploeg RJ, Hunter JP. A systematic review to identify whether perfusate biomarkers produced during hypothermic machine perfusion can predict graft outcomes in kidney transplantation. Transpl Int. 2020;33(6):590-602.
24. Parente A, Osei-Bordom DC, Ronca V, Perera M, Mirza D. Organ Restoration With Normothermic Machine Perfusion and Immune Reaction. Front Immunol. 2020;11:565616.
25. Op den Dries S, Karimian N, Westerkamp AC, Sutton ME, Kuipers M, Wiersema-Buist J, et al. Normothermic machine perfusion reduces bile duct injury and improves biliary epithelial function in rat donor livers. Liver Transpl. 2016;22(7):994-1005.
26. Liu Q, Nassar A, Farias K, Buccini L, Baldwin W, Mangino M, et al. Sanguineous normothermic machine perfusion improves hemodynamics and biliary epithelial regeneration in donation after cardiac death porcine livers. Liver Transpl. 2014;20(8):987-99.
27. Bral M, Aboelnazar N, Hatami S, Thiesen A, Bigam DL, Freed DH, et al. Clearance of transaminases during normothermic ex situ liver perfusion. PLoS One. 2019;14(4):e0215619.
28. Bhogal RH, Mirza DF, Afford SC, Mergental H. Biomarkers of Liver Injury during Transplantation in an Era of Machine Perfusion. International journal of molecular sciences. 2020;21(5):1578.
29. Hosgood SA, Barlow AD, Hunter JP, Nicholson ML. Ex vivo normothermic perfusion for quality assessment of marginal donor kidney transplants. Br J Surg. 2015;102(11):1433-40.
30. Baranger J, Mertens L, Villemain O. Blood Flow Imaging with Ultrafast Doppler. J Vis Exp. 2020(164).
31. Tabrizchi R, Pugsley MK. Methods of blood flow measurement in the arterial circulatory system. J Pharmacol Toxicol Methods. 2000;44(2):375-84.
32. Rother U, Gerken ALH, Karampinis I, Klumpp M, Regus S, Meyer A, et al. Dosing of indocyanine green for intraoperative laser fluorescence angiography in kidney transplantation. Microcirculation. 2017;24(8).
33. De Backer D, Donadello K, Cortes DO. Monitoring the microcirculation. J Clin Monit Comput. 2012;26(5):361-6.
34. EASL Clinical Practice Guidelines: Liver transplantation. J Hepatol. 2016;64(2):433-85.
35. Rodríguez Faba O, Boissier R, Budde K, Figueiredo A, Taylor CF, Hevia V, et al. European Association of Urology Guidelines on Renal Transplantation: Update 2018. Eur Urol Focus. 2018;4(2):208-15.
36. Wells WA, Thrall M, Sorokina A, Fine J, Krishnamurthy S, Haroon A, et al. In Vivo and Ex Vivo Microscopy: Moving Toward the Integration of Optical Imaging Technologies Into Pathology Practice. Arch Pathol Lab Med. 2019;143(3):288-98.
37. Uz Z, Shen L, Milstein DMJ, van Lienden KP, Swijnenburg RJ, Ince C, et al. Intraoperative Imaging Techniques to Visualize Hepatic (Micro)Perfusion: An Overview. Eur Surg Res. 2020;61(1):2-13.
38. Luker GD, Luker KE. Optical imaging: Current applications and future directions. Journal of Nuclear Medicine. 2008;49(1):1-4.

39. Jacques SL. Optical properties of biological tissues: a review. Phys Med Biol. 2013;58(11):R37-61.
40. Schuh S, Holmes J, Ulrich M, Themstrup L, Jemec GBE, De Carvalho N, et al. Imaging Blood Vessel Morphology in Skin: Dynamic Optical Coherence Tomography as a Novel Potential Diagnostic Tool in Dermatology. Dermatol Ther (Heidelb). 2017;7(2):187-202.
41. Feng W, Shi R, Zhang C, Liu S, Yu T, Zhu D. Visualization of skin microvascular dysfunction of type 1 diabetic mice using in vivo skin optical clearing method. J Biomed Opt. 2018;24(3):1-9.
42. Anderson ME, Moore TL, Lunt M, Herrick AL. Digital iontophoresis of vasoactive substances as measured by laser Doppler imaging--a non-invasive technique by which to measure microvascular dysfunction in Raynaud's phenomenon. Rheumatology (Oxford). 2004;43(8):986-91.
43. Al-Allaf AW, Khan F, Moreland J, Belch JJ, Pullar T. Investigation of cutaneous microvascular activity and flare response in patients with fibromyalgia syndrome. Rheumatology (Oxford). 2001;40(10):1097-101.
44. Teeuwen T. Optical methods to image and measure microcirculation or mitochondrial metabolism during local circulatory arrest and reperfusion: Review of their potential in transplant surgery. 2022.
45. Briers D, Duncan DD, Hirst E, Kirkpatrick SJ, Larsson M, Steenbergen W, et al. Laser speckle contrast imaging: theoretical and practical limitations. J Biomed Opt. 2013;18(6):066018.
46. Bezemer R, Klijn E, Khalilzada M, Lima A, Heger M, van Bommel J, et al. Validation of near-infrared laser speckle imaging for assessing microvascular (re)perfusion. Microvasc Res. 2010;79(2):139-43.
47. Liss AG, Liss P. Use of a modified oxygen microelectrode and laser-Doppler flowmetry to monitor changes in oxygen tension and microcirculation in a flap. Plast Reconstr Surg. 2000;105(6):2072-8.
48. Kernick DP, Tooke JE, Shore AC. The biological zero signal in laser Doppler fluximetry - origins and practical implications. Pflugers Arch. 1999;437(4):624-31.
49. Binzoni T, Humeau-Heurtier A, Abraham P, Mahe G. Blood perfusion values of laser speckle contrast imaging and laser Doppler flowmetry: is a direct comparison possible? IEEE Trans Biomed Eng. 2013;60(5):1259-65.
50. Jöbsis FF. Noninvasive, infrared monitoring of cerebral and myocardial oxygen sufficiency and circulatory parameters. Science. 1977;198(4323):1264-7.
51. McCormick PW, Stewart M, Goetting MG, Dujovny M, Lewis G, Ausman JI. Noninvasive cerebral optical spectroscopy for monitoring cerebral oxygen delivery and hemodynamics. Crit Care Med. 1991;19(1):89-97.
52. Kim MB, Ward DS, Cartwright CR, Kolano J, Chlebowski S, Henson LC. Estimation of jugular venous O2 saturation from cerebral oximetry or arterial O2 saturation during isocapnic hypoxia. J Clin Monit Comput. 2000;16(3):191-9.
53. Hongo K, Kobayashi S, Okudera H, Hokama M, Nakagawa F. Noninvasive cerebral optical spectroscopy: depth-resolved measurements of cerebral haemodynamics using indocyanine green. Neurol Res. 1995;17(2):89-93.
54. Ince C. Sidestream dark field imaging: an improved technique to observe sublingual microcirculation. Crit Care. 2005;9(Suppl 1):P72.
55. Heeman W, Maassen H, Calon J, van Goor H, Leuvenink H, van Dam GM, et al. Real-time visualization of renal microperfusion using laser speckle contrast imaging. J Biomed Opt. 2021;26(5).
56. O'Doherty J, McNamara P, Clancy NT, Enfield JG, Leahy MJ. Comparison of instruments for investigation of microcirculatory blood flow and red blood cell concentration. J Biomed Opt. 2009;14(3):034025.
57. Gardner AW, Parker DE, Webb N, Montgomery PS, Scott KJ, Blevins SM. Calf muscle hemoglobin oxygen saturation characteristics and exercise performance in patients with intermittent claudication. J Vasc Surg. 2008;48(3):644-9.
58. Glader BE, Sullivan DW. Erythrocyte disorders leading to potassium loss and cellular dehydration. Prog Clin Biol Res. 1979;30:503-13.

59. Ponder E. Accumulation of potassium by human red cells. J Gen Physiol. 1950;33(6):745-57.
60. Yang J. Anticoagulant Citrate Phosphate Dextrose Adenine Solution. USP2019.
61. Lignell S, Lohmann S, Rozenberg KM, Leuvenink HGD, Pool MBF, Lewis KR, et al. Improved Normothermic Machine Perfusion After Short Oxygenated Hypothermic Machine Perfusion of Ischemically Injured Porcine Kidneys. Transplant Direct. 2021;7(2):e653.
62. Pool MBF, Hamelink TL, van Goor H, van den Heuvel MC, Leuvenink HGD, Moers C. Prolonged ex-vivo normothermic kidney perfusion: The impact of perfusate composition. PLoS One. 2021;16(5):e0251595.
63. Sturesson C, Milstein DM, Post IC, Maas AM, van Gulik TM. Laser speckle contrast imaging for assessment of liver microcirculation. Microvasc Res. 2013;87:34-40.
64. Bezemer R, Legrand M, Klijn E, Heger M, Post IC, van Gulik TM, et al. Real-time assessment of renal cortical microvascular perfusion heterogeneities using near-infrared laser speckle imaging. Opt Express. 2010;18(14):15054-61.
65. Venema LH, Brat A, Moers C, t Hart NA, Ploeg RJ, Hannaert P, et al. Effects of Oxygen During Long-term Hypothermic Machine Perfusion in a Porcine Model of Kidney Donation After Circulatory Death. Transplantation. 2019;103(10):2057-64.
66. Horváth T, Jász DK, Baráth B, Poles MZ, Boros M, Hartmann P. Mitochondrial Consequences of Organ Preservation Techniques during Liver Transplantation. Int J Mol Sci. 2021;22(6).